

An overview of flow features and mixing in micro T and arrow mixers

Simone Camarri,[†] Alessandro Mariotti,[†] Chiara Galletti,[†] Elisabetta Brunazzi,[†]

Roberto Mauri,[†] and Maria Vittoria Salvetti^{*,†,‡}

[†]*Dipartimento di Ingegneria Civile e Industriale, University of Pisa, Pisa, Italy*

[‡]*corresponding author*

E-mail: maria.vittoria.salvetti@unipi.it

Phone: +39 050 2217262

Abstract

An overview of the mixing performances of micro T-mixers operating with a single fluid is presented. The focus is on the relationship between flow features and mixing. Indeed, T-mixers are characterized by a variety of regimes for increasing Reynolds numbers; they are briefly described, in particular in terms of the three-dimensional vorticity field, which can explain the different mixing performances. The effects of changes in the aspect ratios of the channels are also reviewed. The role of instability and sensitivity analyses in highlighting the mechanisms of onset of the different regimes is then described. These analyses also suggest possible geometrical modifications to promote mixing. We focus on that consisting in the downward tilting of the inlet channels (arrow-mixers). Arrow-mixers are interesting because the onset of the engulfment regime is anticipated at lower Reynolds numbers. Hence, the mixing performances of arrow-mixers with varying Reynolds number are described.

Introduction

Microfluidic devices are receiving large attention for the intensification of many processes in fine-chemistry, pharmaceutical and food industries. Micro-reactors ensure a continuous operation with an unprecedented control over operating conditions, and thus product quality. The very large surface-to-volume ratio allows extremely high heat transfer rates to be achieved, thus opening the possibility to deal with very exothermic reactions without the need of diluting the reactants. Indeed some reaction pathways, too dangerous to be run in stirred vessels, could be successfully conducted in micro-reactors. This is the case, for instance, of the direct fluorination of aromatics with elemental fluorine¹ and of the synthesis of trinitroglycerin, which can be run in micro-reactors at relatively high temperatures, thus improving productivity². In addition, the scale-up of the synthetic route from the laboratory to the production scale is not necessary as the desired production rate can be achieved through a numbering-up of the micro-reactors, often assembled in modular systems. Roberge et al.³ analyzed different types of reactions for the synthesis of drugs and fine chemicals; these authors estimated that around 50% of the homogeneous and 30% of the heterogeneous reactions would benefit of being conducted in micro-reactors.

Moreover, micro-reactors are gathering interest for the production of nano- and micro-particles, that may be generated with unprecedented control on particle shape and dimensions, even leading to specifically shaped or mono-disperse particles, and minimizing unwanted products and wastes⁴. In this field, one of the most promising applications is the production of drug-embedding polymer particles⁵. This process is based on the solvent displacement technique, where a solvent embedding the polymer molecules and the drug is mixed with another liquid which acts as a non-solvent for the polymer. The rapid interdiffusive mixing of solvent and non-solvent leads the local composition of the suspending solution to swiftly pass through the critical precipitation condition, thus promoting nucleation over particle growth.

Despite the above important benefits and the abundance of many convincing results

described in literature, the actual implementation of micro-reactors for applications in a commercial setting has been surprisingly limited so far. One of the reasons is that, while the process miniaturization is essential to generate key functionalities, such as the high heat transfer rate, it however leads to a very low mixing efficiency, due to the fact that the flow is laminar, with low Reynolds numbers, so that mixing occurs by diffusion only. Since the diffusion time is $\tau_{diff} = \ell^2/D$, a typical small molecule with diffusivity $D = 10^{-9} \text{ m}^2/\text{s}$ needs $\tau_{diff} = 10 \text{ s}$ to diffuse across a small length of $\ell = 100 \mu\text{m}$. A large molecule (often involved in pharmaceutical and fine chemistry processes) has a typical diffusivity $D = 10^{-11} \text{ m}^2/\text{s}$ and so it needs $\tau_{diff} = 1000 \text{ s}$ to diffuse across a small length of $\ell = 100 \mu\text{m}$. Hence, the length needed to span this residence time to achieve mixing is $\ell_{mix} = U\tau = \ell Pe$ where Pe is the Peclet number, i.e., $Pe = \tau_{diff}/\tau_{conv} = U\ell/D$, which thus depends on both Schmidt, Sc and Reynolds, Re , numbers. Since the typical Schmidt number for aqueous solutions is $Sc = \frac{\mu}{\rho D} = 400\text{--}2500$, so $Sc = \mathcal{O}(10^3)$, the resulting length to achieve mixing is $\ell_{mix} \approx 10^3 Re \ell$. Considering reasonable production rates, so that $Re = \mathcal{O}(10\text{--}10^2)$, we obtain $\ell_{mix} \approx 10^4\text{--}10^5 \ell$. Hence, if mixing occurs purely due to diffusion, the channel length must be thousands of times larger than the channel height to achieve a significant mixing of the two streams in the mixing channel. This is why many micro-reactors present a confluence region, where the reactants are fed, and then a very long region, often like a serpentine, which is devoted to letting reaction occur.

In order to have more compact micro-devices, methods to enhance mixing are needed in the absence of turbulence. These methods are classified into active and passive⁶⁻⁸. The former ones use external energy sources to generate disturbances (e.g. pressure, electro-dynamics, magneto-hydrodynamics, acoustic and thermal) in the flow, thus improving mixing. Instead, passive methods are based on a special geometrical configuration of the devices aimed at exploiting the flow topology and structures to promote mixing⁹. These micro-reactors can be further classified according to the underlying principle, as lamination (e.g. T and Y mixers, split/recombine configurations¹⁰), chaotic advection (e.g. serpentine, zigzag),

Coanda, etc...

Passive micro-devices are very appealing, as they are easier to fabricate and more robust than active mixers, and, of course, do not need external energy to be operated. Their performance strongly depends on the flow behavior, so that the optimization of these devices requires a better comprehension of the fluid dynamics at the microscale.

Indeed, the flow behavior influences mixing of reactants and in turn, reaction yield. This is also important in the presence of nanoparticle precipitation, because solvents and non-solvents are typically completely miscible with one another in the entire range of composition.

The present paper is intended to provide a review of the flow regimes occurring in a T-shaped micro-mixer (see the sketch in Figure 1). This mixer represents the simplest passive mixer and it is also interesting as it may be found as a junction element in more complex micro-reactor networks. Many modifications of this basic geometry have been proposed in the literature, as for instance configurations in which the inlets are not aligned to induce a spiral motion in the confluence region¹¹. Some works focused instead on T-jets, which are characterized by a headspace between the location at which the inlet streams join the mixing channel and the mixing channel top wall. The presence of such a head above the injectors may affect the mixing efficiency. An overview of steady and unsteady regimes occurring in T-jets and of their sensitivity to geometrical parameters is provided by Sultan et al.^{12,13}. Other possible variations of this basic T-mixer may deal with different cross-sections other than square or rectangular (see e.g.^{14,15}). All these modifications will not be taken into account in the present work that will focus instead on T-shaped micro-mixers with square or rectangular cross-sections. Moreover, for the sake of brevity, the overview is limited to mixers operating with a single liquid. For the effects of varying viscosity and density we refer for instance to¹⁶⁻²⁰. Despite its geometrical simplicity and the assumption of a single fluid, the flow dynamics is really complex with several flow regimes impacting on the degree of mixing. The scenario is further complicated by the effect of a few geometrical parameters, such as the aspect ratio. The focus is on the link between flow topology/dynamics and mixing. Indeed,

understanding the mechanisms triggering the different flow regimes is fundamental to the control of the mixing process and to devise strategies to optimize reaction yields. We show herein how this optimization may be achieved, for instance, through techniques like stability and sensitivity analysis, which allow the mechanisms inducing the onset of the instability leading to the different flow regimes to be identified. For instance, this kind of analysis suggests a simple geometrical modification which can significantly influence the onset of regimes characterized by efficient mixing, i.e., a downward tilting of the axes of the inlet channels with respect to the one of the mixing channel leading to arrow-shaped mixers. The flow regimes and mixing performances in arrow-mixers are also reviewed herein.

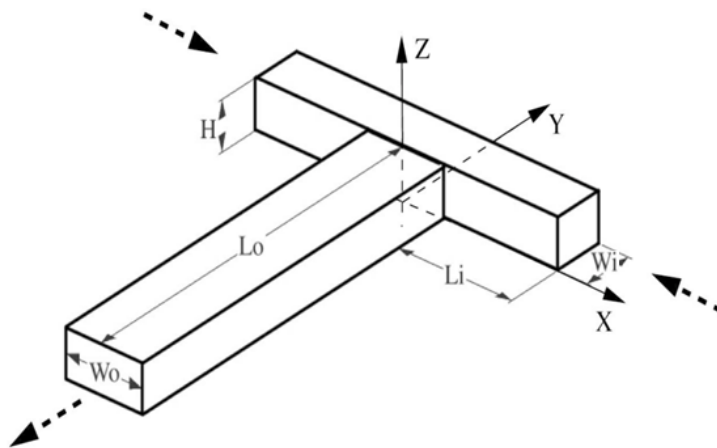


Figure 1: Sketch of a T-mixer. H denotes the mixer depth, W_i the width of the inlet channels, W_o the width of the mixing channel, L_i the length of the inlet channels and L_o the length of the mixing channel. X , Y and Z indicate the coordinates in the three directions shown in the figure made non-dimensional by using the hydraulic diameter of the mixing channel.

Flow regimes and mixing in T-mixers

In spite of the simple geometry, experimental and numerical studies in the literature have shown that significantly different flow regimes and features can be present in T-mixers and have pointed out their remarkable effects on mixing, also when the mixers operate with a single fluid having constant properties. The most important parameter which determines

the occurrence of a flow regime is the Reynolds number, defined as $Re = \frac{UL}{\nu}$, where U and L are a characteristic velocity and length respectively and ν is the kinematic viscosity of the working fluid. In the present paper, unless differently specified, Re is based on the bulk velocity, U_b and on the hydraulic diameter of the mixing channel, d_h . Moreover, we focus on a single fluid having Newtonian properties, and thus ν is constant. Besides the Reynolds number, the onset and appearance of the different regimes may vary with geometrical and flow parameters, such as the aspect ratio and shape of the channel cross sections, or the inlet flow conditions. In the present section, unless differently specified, we mostly focus on T-mixers having square inlet cross-sections, a mixing channel having a cross-section area twice that of the inlet channels (constant U_b) and fully-developed inlet velocity profiles. The effects of the inlet cross section geometry, and, in particular of its aspect ratio, are examined in the next section, as well as those of flow acceleration and deceleration in the mixing channel. For the influence of inflow boundary conditions we refer, e.g., to Galletti et al.²¹ or to Schikarski et al.²² for higher Reynolds numbers and transition to turbulence.

Let us describe now what happens by progressively increasing the Reynolds number. For very low Reynolds numbers, the two inlet streams remain completely segregated in the mixing channel (*stratified* or *segregated* or *laminar* regime). In this case, mixing is only due to diffusion, and thus, as previously discussed in the Introduction, the mixing efficiency is very low.

By increasing the Reynolds number, the first change in flow topology is observed with the onset of the so-called *vortical* regime, which is characterized by the presence of well defined vortical structures steady in time. The vortical regime was firstly observed and described in the numerical simulations by Kockmann et al.^{23,24} and in the simulations and experiments by Engler et al.²⁵ and Wong et al.²⁶. In particular, Kockmann et al.²⁴ pointed out the presence of steady symmetrical vortex pairs at the entrance of the mixing channel; nonetheless, the flow streams were found to remain segregated in the mixing channel. They attributed this behavior to the fact that the vortical structures are rapidly damped by viscous

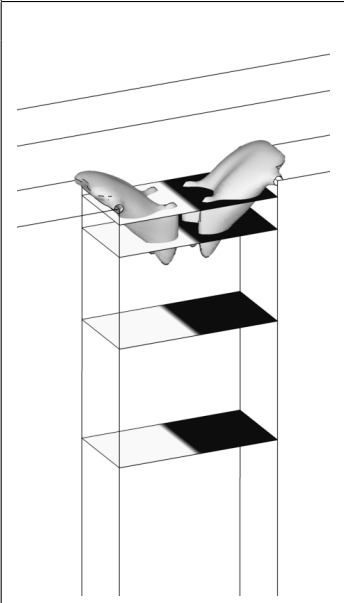
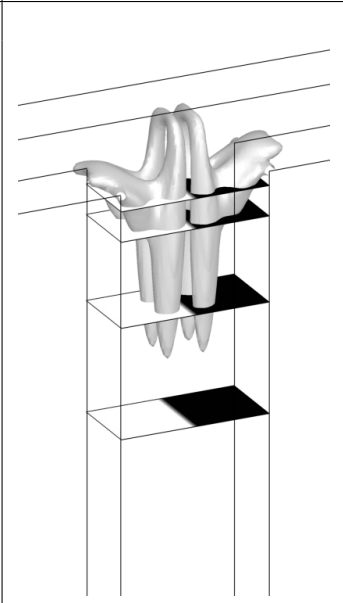
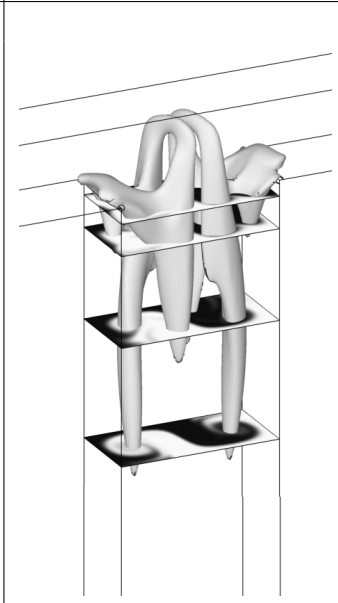
forces. Similar features were also observed by Bothe et al.²⁷ and by Dreher et al.²⁸. Later on, Hussong et al.^{29, 30} and Fani et al.³¹ identified in their numerical simulations the presence of two steady 3D vortical structures, which are almost U-shaped, formed by a top part located at the confluence of the two streams and by two counter-rotating legs in the mixing channel. Unlike what is stated in Kockmann et al.²³, the two couples of counter rotating vortices are found to persist in the mixing channel, especially for higher Re ; however, they are perfectly symmetric, and thus the flow field displays the two reflectional symmetries of the mixer geometry (see e.g. Table 1). Consequently, also in this regime mixing occurs only by diffusion and the mixing efficiency remains low. This topology has been confirmed by more recent works³²⁻³⁴. Note that in Table 1, as in some following tables and figures, the λ_2 -criterion³⁵ is used to identify the vortical structures. According to this criterion, a vortex is defined as a connected fluid region where the second largest eigenvalue of the symmetric tensor $\mathbf{L} = \mathbf{S} \cdot \mathbf{S} + \mathbf{A} \cdot \mathbf{A}$ is negative, i.e. $\lambda_2 < 0$. Here, \mathbf{S} and \mathbf{A} indicate the strain rate and vorticity tensors, i.e. the symmetric and anti-symmetric part of the velocity gradient, $\nabla \mathbf{u}$. As for the physical mechanisms leading to the formation of the observed 3D vortices (also called Dean vortices), Hussong et al.²⁹ identified as a key element the flow separations occurring at the corners at the inlet of the mixing channel. Conversely, Fani et al.³¹ pointed out the importance of the two flow recirculation regions forming near the top wall at the confluence of the two inlet streams, from which the top parts of the 3D vortical structures originate. The two legs of each structure are simply the effect of vorticity convection in the mixing channel; the vorticity formed at the mixing-channel corner is indicated to play only a minor role. Note that the simulations in Fani et al.³¹ were carried out for inlet rectangular cross sections having $\frac{W_i}{H} = 0.75$; however, Andreussi et al.³² showed that the flow features in the vortical regime are the same as for a T-mixer operating in the same conditions and with square inlet cross sections. The precise quantification of the value of Re at which the vortical regime takes place has not received much attention in the literature, probably because this regime is not interesting from the viewpoint of mixing. Therefore, a quite large range of

values is given, e.g. $5-10$ ^{34,36}, $40-50$ ^{25,37-39} or 80 ^{33,40}.

By further increasing the Reynolds number, over a critical value, Re_{StAsym} , we enter into the so-called *engulfment* or *steady asymmetric* regime, which has been widely studied in the literature. In this regime, the flow symmetries are broken and the mixing efficiency dramatically increases. Therefore, the engulfment regime is the first one having a remarkable practical interest. As for the vortex one, the engulfment regime was firstly observed and described by Kockmann et al.^{23,24} and by Engler et al.²⁵ and slightly later by Bothe et al.²⁷. The key features identified in all these works are the loss of the double reflectional symmetry of the flow, the presence of two strong co-rotating vortical structures in the mixing channel and the fact that each inlet fluid stream reaches the opposite wall in the mixing channel. Kockmann et al.²⁴ analyzed in more detail the flow in terms of streamlines. They identified three key regions in the flow, namely a stagnation region near the mixer top wall, a pair of small vortices near the mixing channel entrance and a couple of larger vortex regions more downstream in the mixing channel, and they suggested that mixing enhancement is mainly obtained by the stretching of the fluid elements in the first two regions. A few further studies^{27,39} also interpreted the enhanced mixing performance in the engulfment regime in terms of augmented contact area between the two streams. Based on the analysis previously described for the vortical regime, Hussong et al.²⁹ and Fani et al.³¹ and more recent works^{32,33} investigated the engulfment regime in terms of the 3D vortical structures. In all these works, it is observed that, because of the loss of symmetry in the top part of the channel, one of the two legs of each vortical structure is more fed by the incoming fluid than the other; therefore, the two strongest legs, which are co-rotating, survive far downstream in the mixing channel, while the two weaker legs rapidly disappear (see e.g. Table 1). This explains the two co-rotating vortices in the mixing channel and the related S-shaped flow pattern in the passive scalar concentration isocontours, characteristic of the engulfment regime. The enhancement of the mixing efficiency can be also explained by the velocity induced by this couple of co-rotating vortices, which helps the mixing between the two streams through convection. Fani

et al.³¹, once again, pointed out the importance of the loss of the symmetry of recirculating regions at the confluence of the inlet streams leading to the tilting of the top parts of the 3D vortical structures, which is in turn responsible of the previously described asymmetry of the legs and of the related flow features in the mixing channel. The key role of the flow recirculations near the top wall is confirmed also by the analysis of the instability mechanisms leading to the onset of the engulfment regime (see the following dedicated section). As for the value of the critical Reynolds number for the onset of the engulfment regime, a good agreement is found in the literature, with $Re_{StAsym} = 138-155$ ^{25,32,33,36,37,39-41}.

Table 1: Summary of the steady flow regimes as from the numerical isosurfaces of the vortex indicator λ_2 from Mariotti et al.³³. The passive scalar concentration at different cross-sections in the mixing channel is also shown. Adapted with permission from Mariotti et al.³³. Copyright 2018 Elsevier B.V.

Stratified regime ($Re < 80$)	Vortex regime ($Re = 80-140$)	Engulfment regime ($Re = 145-220$)
		

The previously described flow regimes are all steady in time. Clearly, flow unsteadiness can be induced by time-dependent boundary conditions or external perturbations or they naturally arise when the flow undergoes transition to turbulence. However, it has been observed that periodic oscillations of the flow can be present also without any external per-

turbation for Reynolds numbers lower than the critical one of transition to turbulence, i.e. still in laminar conditions. A first hint of the flow becoming unsteady when the Reynolds number is moderately increased after the onset of the engulfment regime was given in the experimental work by Hoffmann et al.³⁹, while Bothe et al.²⁷ reported a periodic behavior in their simulations for $Re > 240$ and using a fine grid resolution. The first numerical study on unsteady periodic regimes can be found in Dreher et al.²⁸. They identified a periodic pulsating flow for $240 < Re < 400$. Such periodic pulsations were found to disappear when $Re > 500$, when a turbulent chaotic motion was observed. Dreher et al.²⁸ linked the velocity and concentration periodic oscillations to pulsating vortices flowing through the mixing channel and they attributed the periodic formation of such vortices to Kelvin-Helmholtz instabilities of the shear layers in the top part of the mixer at the confluence between the two streams. This conjecture is based on the visualizations of the scalar concentration in planes normal to the axis of the mixing channel in the top part of the mixer, which show patterns very similar to Kelvin-Helmholtz instabilities of shear layers (see, e.g., Figure 2 taken from Fani et al.⁴²). Dreher et al.²⁸ also reported experimental visualizations which corroborate their numerical results. The first systematic experimental investigations of unsteady regimes in T-mixers can be found in Thomas and Ameel⁴³ and Thomas et al.⁴⁴. In agreement with Dreher et al.²⁸, for $260 \leq Re < 460$, they observed two or four vortical structures periodically forming at the T-channel junction, which they also attributed to the roll-up of the shear layers present in this zone, and the generation of periodic coherent waveforms in the mixing channel. This regime, which was called by Thomas and Ameel⁴³ *unsteady asymmetric*, was also observed and investigated in more recent numerical and experimental works^{21,22,30,32,33,42,45,46}. In particular, Fani et al.⁴² gave a physical interpretation of this regime in terms of the dynamics of 3D vortical structures, which are similar to those also present in the steady engulfment regime previously described. In the unsteady asymmetric regime, these structures undergo a cyclic behavior: first, the two top parts approach each other. As they move closer, their tilting angle rapidly increases up to a maximum value, at

which the top parts and the strong legs of the two vortical structures merge. The top parts, containing vorticity of opposite sign, annihilate after merging, while the strong legs create a blob of vorticity, which is quickly convected towards the mixing channel; starting from this moment the legs are not fed anymore and their intensity quickly decreases. At the same time, two new 3D structures of the same type form and are convected towards the symmetry plane, where they will replace the original two vortical structures. The cycle then starts again. A couple of representative instants during the cycle are shown in Table 2; as for the dynamics of the vortex top parts we refer to Fig.6 of Fani et al.⁴². The co-rotating vortices resembling a Kelvin-Helmholtz instability, observed on the $x - z$ planes at the interface between the two streams, are actually the traces of the 3D vortical structures during the cycle. This scenario was confirmed by the stability analysis in Fani et al.⁴² (also presented in the following) and in more recent studies^{32,33,46}. The unsteady asymmetric regime is interesting from a practical viewpoint because it is characterized by a larger mixing than the engulfment one^{28,46}. In particular, Mariotti et al.⁴⁶ showed that the periodic shedding of a vorticity blob in the mixing channel gives a remarkable contribution to mixing. As for the critical value of the Reynolds number at which this regime occurs, the following range is found in the literature^{27,28,30,32,33,43,46} : $Re_{UnstAsym} = 180-240$.

For larger Reynolds numbers, $Re \geq 350$, Thomas and Ameel⁴³ found that the flow remains unsteady, but it is mostly characterized by a symmetric four-vortex topology, in which the stagnation point oscillates, while losses of symmetry only intermittently occur in the flow. Clearly, they found this latter regime, called *unsteady symmetric regime*, detrimental to mixing. More recent studies^{32,33,42,46} confirmed the presence of this regime and the associated drop of mixing and they found that the flow unsteadiness is due to a periodic rotation or translation of the top parts of the 3D vortical structures, which, however, for most of the time remain very similar to those encountered in the vortex regime (see e.g. Table 2).

Different ways have been used in the literature to quantify mixing. Most of them^{13,20,25,28,30,37,46-48} are based on the definition of an index, called mixing intensity, mixing efficiency or mixing

degree, in the following form:

$$\delta_m = 1 - \sqrt{I_S}$$

where I_S is an index of the segregation between the two streams. The definition of I_S may be different among the studies in the literature, as well as the location in the mixing channel at which δ_m is computed. We refer to the above cited papers for more details. In any case, δ_m varies between 0 and 1, being $\delta_m = 0$ and $\delta_m = 1$ for completely segregated and fully mixed flows, respectively. Other indicators may be the mixing time²² or the potential of diffusive mixing³⁹. An example of quantification of the mixing performances is given in Fig. 3, showing the degree of mixing δ_m vs. Re obtained in the simulations in Mariotti et al.⁴⁶ for all the flow regimes previously described. The first sudden increase corresponds to the onset of the engulfment regime and has been observed in many previous works (see the references above). By further increasing Re , the degree of mixing keeps monotonically increasing, with a larger growth rate when entering the unsteady asymmetric regime. When the flow is unsteady, the symbols show the degree of mixing averaged over a cycle, while the bars indicate the fluctuations within the cycle. The drop of δ_m at $Re \simeq 325$ corresponds to the onset of the unsteady symmetric regime. This drop was also observed in the simulations of Dreher et al.²⁸ and it is consistent with the discussion in the experimental work of Thomas and Ameel⁴³. Also note how in this latter regime, not only the cycle-averaged values of δ_m are much lower than those observed in the engulfment and unsteady asymmetric ones, but also the time fluctuations are very low, indicating thus limited effects of flow unsteadiness on mixing in this regime.

Figure 4 compares the values of the Strouhal number, $St = fd_h/U_b$, i.e. the characteristic frequency, f , made non-dimensional by U_b and d_h , found in the unsteady regimes in experiments and simulations in the literature. Some dispersion can be noticed among the different sets of data. **In the experiments, the dispersion may be related to small differences in the set-up, which can not be controlled or even detected, such as a small unbalance of the flow rate in the two streams, some unsteadiness in the inlet flow or geometrical imperfections**

due to manufacturing tolerances. On the other hand, in numerical simulations dispersion may be due to differences in boundary conditions, as e.g. in the inlet velocity profile shape, or in the length of inlet and outlet channels, as well as in grid resolution, time step size and numerical method. However, in all cases St increases monotonically in both asymmetric and symmetric periodic regimes, while a sudden variation of St is observed at the transition between the two periodic regimes. Mariotti et al.⁴⁶ also investigated which are the proper scaling factors to obtain a non-dimensional frequency independent of Re within each regime. They found that the rotation angular velocity of the top parts of the 3D vortical structures is the proper scaling factor in the unsteady asymmetric periodic regime, whereas its mean lateral displacement velocity can be used in the unsteady symmetric periodic regime together with a geometrical reference length. This shows that the characteristic time-scales are linked to the dynamics of the top parts of the 3D vortical structures present in the mixer.

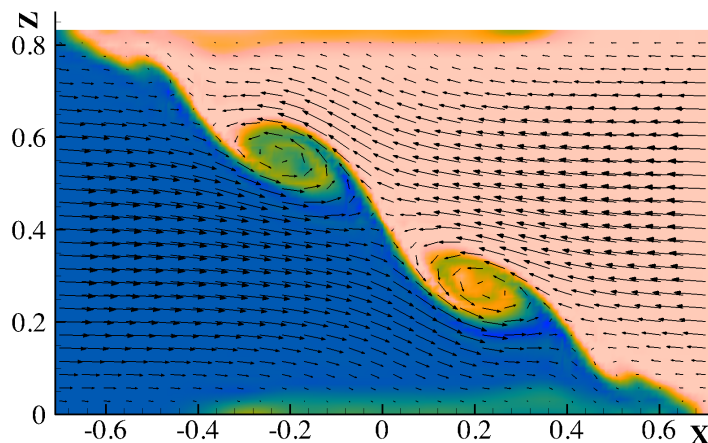


Figure 2: Section at $Y = y/d_h = 0.31$ at $Re = 240$: instantaneous in-plane velocity vectors and distribution of a passive scalar (light color), entering from one channel of the mixer from the simulations in Fani et al.⁴². Adapted with permission from Fani et al.⁴². Copyright 2014 AIP Publishing LLC.

The previously analyzed works are experimental and/or numerical. For the sake of brevity, we do not give details about experimental and numerical techniques; the interested readers are referred to the relevant references. It is worth to remark, however, that

Table 2: Summary of the time-periodic flow regimes as from the numerical isosurfaces of the vortex indicator λ_2 (Mariotti et al.³³). Snapshots refer to $\frac{t}{\tau} = 0$ and $\frac{t}{\tau} = 0.5$, τ being the cycle period. The passive scalar concentration at different cross-sections in the mixing channel is also shown. Adapted with permission from Mariotti et al.³³. Copyright 2018 Elsevier B.V.

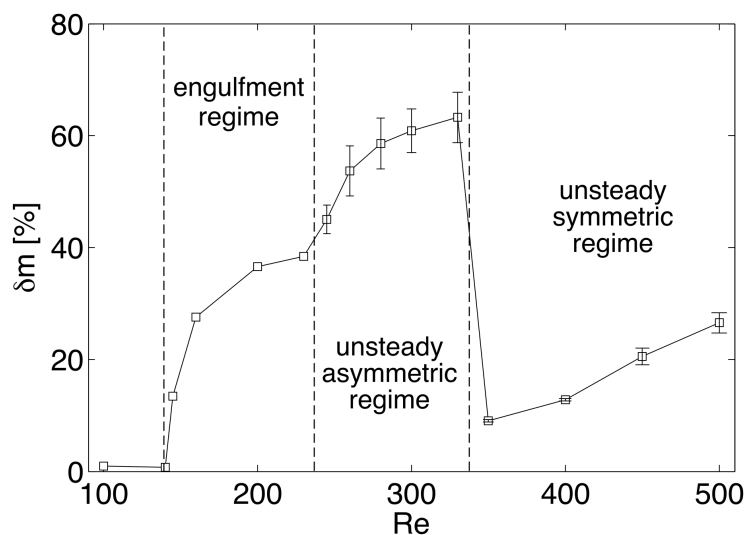
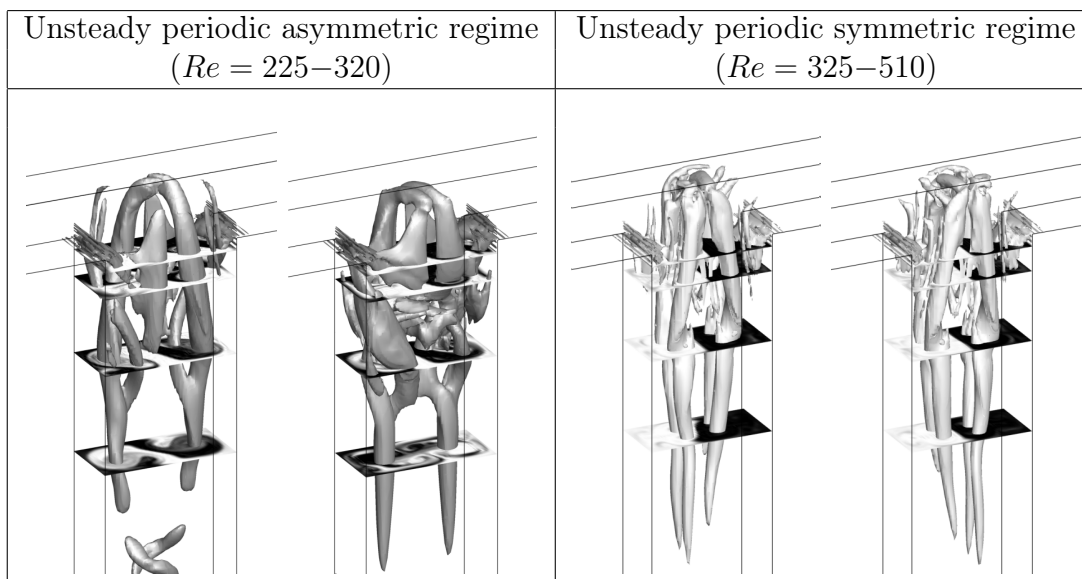


Figure 3: Degree of mixing numerically evaluated at the cross-section $Y = -8$ as a function of the Reynolds number Re from numerical simulations in Mariotti et al.⁴⁶. Adapted with permission from Mariotti et al.⁴⁶. Copyright 2019 American Chemical Society.

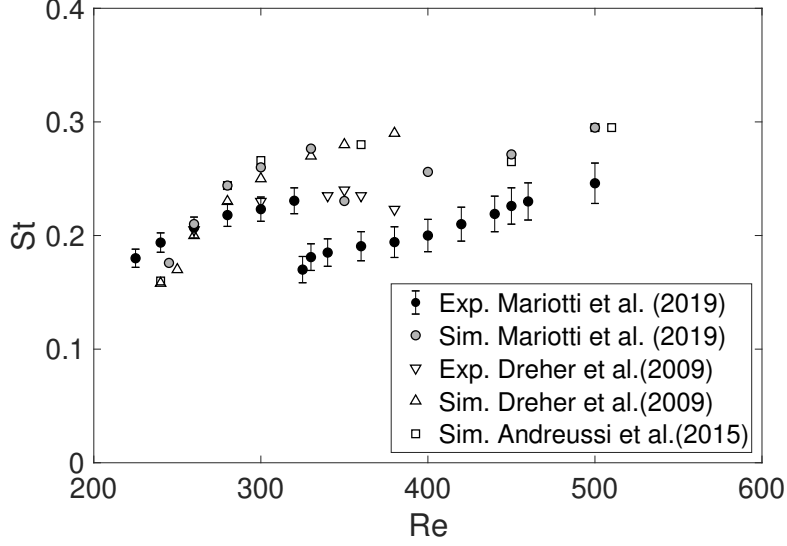


Figure 4: Experimental and numerical Strouhal numbers as a function of the Reynolds number.

numerical simulations, at least up to transition to turbulence, should accurately resolve all the flow relevant features. This implies that the grid resolution should be adequate to accurately capture the smallest flow scales. A critical issue, which remains open, is the resolution needed to accurately compute mixing in liquids. This point is briefly addressed in Appendix.

Effect of aspect ratio

One geometrical parameter that strongly influences the flow regimes, and thus mixing, in T-shaped micro-reactors is the aspect ratio. In particular, two different aspect ratios may be defined for the inlet and the mixing channels, i.e., $\kappa_i = \frac{W_i}{H}$ and $\kappa_o = \frac{W_o}{H}$, respectively. In most of the applications the width of the mixing channel is twice that of the inlet channels, i.e., $W_o = 2W_i$, in order to ensure the same bulk velocities at the inlets and at the outlet. In this case $\kappa_o = 2\kappa_i$ and the flow does not accelerate or decelerate when entering the mixing channel.

Table 3 summarizes the observations in the literature on flow regimes obtained with T-shaped micro-reactors of different aspect ratios κ_i , by reporting the Reynolds numbers at the

onset of the different flow regimes after the vortex one. All cases reported in Table 3 refer to $\kappa_o = 2\kappa_i$ and hence they can be thought as cases where the mixer height H is varied. Here the effect of the aspect ratio will be discussed highlighting differences respect to the reference case of square inlets, i.e., for $\kappa_i = 1$, whose flow regimes have been described in details in the previous section. The first row of Table 3 reports data for the case with square inlets obtained both experimentally and numerically by Mariotti et al.³³. The ranges obtained in the different works in the literature for $\kappa_i = 1$ are given in the previous section.

Table 3: Reynolds numbers at the onset of the different flow regimes for different aspect ratios κ_i and $\kappa_o = 2\kappa_i$. N = the regime does not occur; - = the regime is not investigated; O = the regime is observed but the Re at the onset is not reported; H = hysteresis.

Author	κ_i	Re_{StAsym}	$Re_{UnstAsym}$	$Re_{UnstSym}$	$Re_{Chaotic}$
Mariotti et al. ³³	1	145	225	325	515
Soleymani et al. ⁴⁰	1.66	241.2	-	-	-
Reddy Cherlo and Pushpavanam ⁴⁹	0.5	750	-	-	-
Reddy Cherlo and Pushpavanam ⁴⁹	0.83	300	-	-	-
Poole et al. ⁴¹	0.65	425-600 (H)	-	-	-
Poole et al. ⁴¹	0.675	161	-	-	-
Poole et al. ⁴¹	0.7	154	-	-	-
Poole et al. ⁴¹	0.8	137	-	-	-
Poole et al. ⁴¹	0.833	135	-	-	-
Poole et al. ⁴¹	1.2	153	-	-	-
Fani et al. ^{31,42} Andreussi et al. ³²	0.75	140	220	400	560
Andreussi et al. ³²	2	N	N	420-450 (H)	550
Lobasov et al. ³⁴	2	N ($Re \leq 400$)	-	-	-
Lobasov et al. ³⁴	1.33	180	-	-	-
Lobasov et al. ³⁴	0.8	135	-	-	-
Lobasov et al. ³⁴	0.67	170	-	-	-
Lobasov et al. ³⁴	0.57	N	O	-	-
Lobasov et al. ³⁴	0.5	N	O	-	-
Lobasov et al. ³⁴	0.2	N	O	-	-
Lobasov et al. ³⁴	0.1	N	O	-	-

As it may be observed from Table 3, the aspect ratio affects not only the onset of the different flow regimes, but also their occurrence, as for instance in some cases the engulfment regime may be not even present. In particular, the engulfment regime is observed only for configurations with the inlet channel aspect ratios in the range $0.65 \leq \kappa_i \leq 1.66$ ^{34,41,48}.

Within this range, Fani et al. investigated the morphology of the flow regimes for $\kappa_i = 0.75$, focusing on the symmetry breaking leading to the engulfment regime³¹ as well as on the characterization of the unsteady flow regimes⁴². The features and underlying mechanisms were alike those lately observed for the case of square inlet, i.e., with $\kappa_i = 1$ and discussed in the previous section. For $\kappa_i < 0.65$ the flow undergoes directly the unsteady periodic flow regime immediately after the steady symmetric (vortex) one, as pointed out by Lobasov et al.³⁴. This was attributed to the fact that for low κ_i , i.e., large channel height, the distance between the branches of each U-shaped vortex formed in the vortex regime is too large to allow the interaction between the vortices needed for the onset of the engulfment regime³⁴. A rather weird behavior was observed for $\kappa_i = 0.67$, when the flow firstly undergoes the engulfment regime at $Re_{StAsym} \approx 170$ and subsequently at $Re \approx 250$ it returns back to the vortex regime³⁴. Poole et al.⁴¹ observed that for similar aspect ratios, i.e. at about $\kappa_i \leq 0.65$, there is a significant hysteresis in the determination of Re_{StAsym} , i.e. $Re_{StAsym} = 425-600$. In particular, the numerical results achieved when Re is gradually increased, starting from a steady symmetric (vortex) flow regime, were found to be different from those obtained when Re is gradually decreased from an asymmetric solution. At $\kappa_i = 0.5$ Reddy Cherlo and Pushpavanam⁴⁹ indicated that the engulfment regime occurs at $Re = 750$ in contrast to both Lobasov et al.³⁴ and Poole et al.⁴¹; however a possible reason for such discrepancy could be an insufficient mesh refinement and/or excessive diffusion in the numerical scheme of the former authors⁴¹. The absence of the engulfment regime was also observed for $\kappa_i > 1.66$ ^{32,34} (see Table 3). In particular, for $\kappa_i = 2$, Andreussi et al.³² showed how the flow undergoes directly a transition from the vortex to the unsteady symmetric regime. Moreover, for such large aspect ratio the vortex regime is different from the one observed for $\kappa_i = 1$ and presents a double mirror symmetry with four pairs of main counter-rotating vortices: two strong pairs near the mixing channel axis and two weak pairs far from the axis. Hence the morphology is different from $\kappa_i = 1$, which is characterized by two pairs of counter-rotating vortices. For $\kappa_i = 2$ the mixing channel is so large that the symmetry breaking is hampered; thus no

asymmetric (steady or unsteady) regime can take place. Instead, a direct transition to the unsteady symmetric regime occurs at about $Re_{UnstSym} = 420 - 450$, the exact value being difficult to determine because of the presence of hysteresis. This unsteady symmetric regime is characterized just by small oscillations of the four pairs of vortical legs in the mixing channel, nearly preserving the double mirror symmetry³².

As it may be also observed from Table 3, most of the investigations focused on the determination of the Reynolds number at the onset of the engulfment regime, as this is the regime which allows a rapid increase of the degree of mixing. For the reference case with square inlets, this onset takes place at $Re_{StAsym} = 138 - 155$, as reported in the previous section. Soleymani et al.⁴⁰ suggested a relationship to estimate this critical Reynolds number as a function of the mixer aspect ratios, based on numerical simulations of T-mixers with $\kappa_i = 1 - 2$, most of them presenting acceleration or deceleration effects in the mixing channel as $\kappa_o \neq 2\kappa_i$. The proposed correlation is based on a dimensionless number, called identification number K , which is defined as

$$K = Re^{0.82} \kappa_i^{-0.79} \left(\frac{d_{h,i}}{d_h} \right)^{-1.5} \kappa_o^{0.15} \quad (1)$$

where $d_{h,i}$ is the hydraulic diameter of the inlet channel. According to Soleymani et al.⁴⁰ the engulfment regime occurs for $K \approx 100$, so that Re_{StAsym} may be obtained from the above relationship by substituting this value. However, some authors lately observed that the above correlation can fail for aspect ratios which are outside the range investigated by Soleymani et al.⁴⁰. In particular, Reddy Cherlo and Pushpavanam⁴⁹ showed that the above relationship could lead to a strong underestimation of the critical Reynolds number at the onset of the steady asymmetric regime for $\kappa_i = 0.833$ and $\kappa_i = 0.5$.

Poole et al.⁴¹ observed a good performance of the above relationship for $\kappa_i \geq 1$ but an underestimation of Re_{StAsym} values for smaller κ_i . However such underestimation was not so dramatic as the one pointed out by Reddy Cherlo and Pushpavanam⁴⁹.

Lobasov et al.³⁴ recently proposed a new correlation to predict the critical Reynolds number at the onset of the engulfment regime as a function of the mixing channel width and height.

$$Re_{StAsym} = \left[55 \left(\frac{W_o}{W_{o,ref}} \right)^{-2} + 90 \right] \left[1.95 \left(\frac{H}{H_{ref}} \right)^2 - 4.51 \left(\frac{H}{H_{ref}} \right) + 3.56 \right] \quad (2)$$

where $W_{o,ref}$ and H_{ref} are the reference values of mixing channel width and height, respectively, i.e., $W_{o,ref} = 400\mu\text{m}$ and $H_{ref} = 200\mu\text{m}$ (the reference width of the inlet channel is $W_i = 200\mu\text{m}$). The correlation should be used for $0.5 \leq \frac{W_o}{W_{o,ref}} \leq 5$ and $0.75 \leq \frac{H}{H_{ref}} \leq 1.5$.

All literature data on the onset of the steady asymmetric regime as a function of the inlet channel aspect ratio in case of $\kappa_o = 2\kappa_i$ are shown in Fig. 5 and compared to both relationships of Soleymani et al.⁴⁰ and Lobasov et al.³⁴. The latter correlation provides a good estimation in its range of validity while the correlation of Soleymani et al.⁴⁰ shows some discrepancies for low aspect ratios, as discussed above. The results of Reddy Cherlo and Pushpavanam⁴⁹ strongly overestimate the critical Reynolds number, as already pointed out. When the inlet channel aspect ratio approaches $\kappa_i = 0.65$ there is a rapid increase of the Reynolds needed for the symmetry breaking: for instance $Re_{StAsym} = 425 - 600$ for $\kappa_i = 0.65$ while $Re_{StAsym} = 161$ for $\kappa_i = 0.675$ ⁴¹, consistently with the fact that this is a sort of limit value for the occurrence of the engulfment regime, as previously discussed.

Some investigations focused on the determination of the Reynolds number at the onset of the steady asymmetric regime for T-mixer configurations with $\kappa_o \neq 2\kappa_i$, and thus with acceleration/deceleration effects. These cases are listed in Table 4.

Lobasov et al.³⁴ investigated different mixing channel aspect ratios in the range $\kappa_o = 1 - 10$ using T-mixers with square inlets, i.e., with $\kappa_i = 1$. The authors observed Re_{StAsym} to shift towards smaller Reynolds numbers when increasing κ_o , as reported in Table 4. The degree of mixing augments as well because the contact area between the two fluids increases when increasing the mixing channel width. In addition, Lobasov et al.³⁴ noticed that for

Table 4: Reynolds numbers at the onset of the engulfment (steady asymmetric regime) for different aspect ratios κ_i and κ_o with $\kappa_o \neq 2\kappa_i$. N = the regime does not occur; dec = deceleration effects; acc = acceleration effects.

Author	κ_i	κ_o	type	Re_{StAsym}
Hoffmann et al. ³⁹	1	4	dec.	105
Soleymani et al. ⁴⁰	1.33	5.33	dec.	132
Soleymani et al. ⁴⁰	1	1	acc.	273
Soleymani et al. ⁴⁰	2	2	acc.	477
Reddy Cherlo and Pushpavanam ⁴⁹	0.657	0.657	acc.	N
Reddy Cherlo and Pushpavanam ⁴⁹	1	1	acc.	312
Reddy Cherlo and Pushpavanam ⁴⁹	2	2	acc.	541
Reddy Cherlo and Pushpavanam ⁴⁹	1	0.5	acc.	464
Reddy Cherlo and Pushpavanam ⁴⁹	2	1	acc.	N
Poole et al. ⁴¹	0.657	0.657	acc.	800
Poole et al. ⁴¹	1	1	dec.	252
Poole et al. ⁴¹	2	2	acc.	404
Poole et al. ⁴¹	2	1	acc.	610
Poole et al. ⁴¹	1	0.5	acc.	464
Lobasov et al. ³⁴	1	1	acc.	270
Lobasov et al. ³⁴	1	1.5	acc.	180
Lobasov et al. ³⁴	1	2.5	dec.	125
Lobasov et al. ³⁴	1	3	dec.	110
Lobasov et al. ³⁴	1	3.5	dec.	105
Lobasov et al. ³⁴	1	4	dec.	100
Lobasov et al. ³⁴	1	10	dec.	75

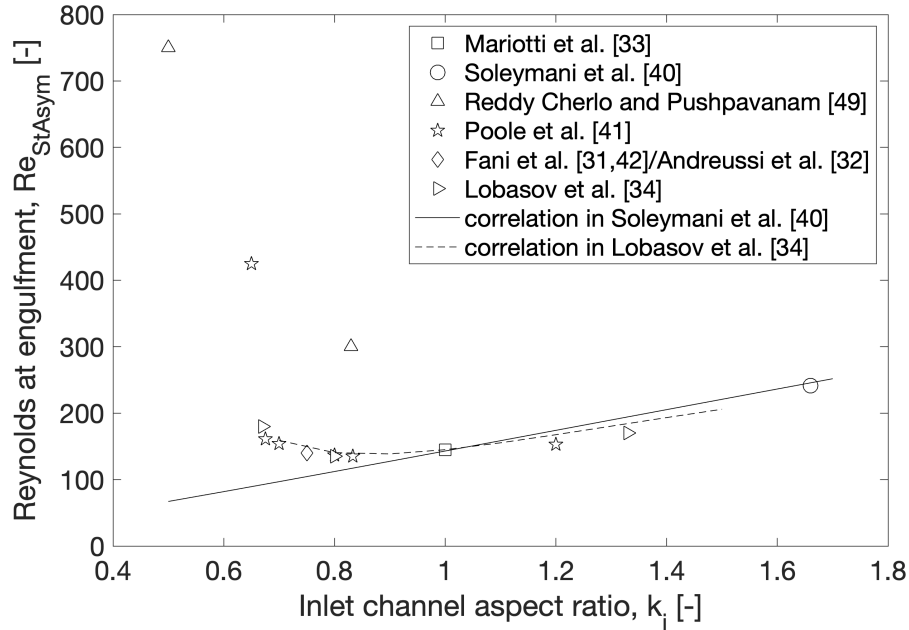


Figure 5: Comparison between values of Reynolds number at the onset of the engulfment regime Re_{StAsym} for different inlet channel aspect ratios κ_i and correlations proposed by Soleymani et al.,⁴⁰ and Lobasov et al.³⁴.

aspect ratios $1.5 \leq \kappa_o \leq 4$ the vortical structures in the engulfment regime were similar to those observed for the reference case (i.e., for $\kappa_o = 2$). In case of deceleration, Hoffmann et al.³⁹, Poole et al.⁴¹ Lobasov et al.³⁴ obtained respectively $Re_{StAsym} = 105$, $Re_{StAsym} = 97$ and $Re_{StAsym} = 100$ for $\kappa_i = 1$ and $\kappa_o = 4\kappa_i$. Soleymani et al.⁴⁸ observed $Re_{StAsym} = 132$ for $\kappa_i = 1.33$ and $\kappa_o = 4\kappa_i$, thus confirming the results of Lobasov et al.³⁴ on the decrease of Re_{StAsym} in case of large κ_o , and thus with deceleration of the flow in the mixing channel. In addition, Lobasov et al.³⁴ highlighted that for large aspect ratios, i.e. for $\kappa_o > 4$, additional vortices were present in the mixing channel, thus further improving mixing.

The case of acceleration was also studied by Soleymani et al.⁴⁸, Poole et al.⁴¹ and Reddy Cherlo and Pushpavanam⁴⁹ who all investigated the case of square inlet and mixing channel cross-sections, i.e., $\kappa_i = 1$ and $\kappa_o = 1$. The onset of the engulfment regime was observed to take place at $Re_{StAsym} \approx 250$ by Soleymani et al.⁴⁸, Poole et al.⁴¹ and Lobasov et al.³⁴, while Reddy Cherlo and Pushpavanam⁴⁹ predicted larger values, i.e., $Re_{StAsym} = 312$. The acceleration in the mixing channel then leads to a delay in the onset of the engulfment

regime. Moreover, Lobasov et al.³⁴ pointed out that in case of a square mixing channel, i.e., for $\kappa_o = 1$, the steady asymmetric regime appears different from the one observed for $\kappa_o = 2$ (and $\kappa_i = 1$). In particular, the two strong vortical legs, which are typical of the engulfment regime, merge into a single vortical structure because of the insufficient space for the expansion of the vortices. Additional investigations using different inlet channel aspect ratios and same cross-sections for the inlet and mixing channels, i.e., $\kappa_o = \kappa_i$, indicated that the engulfment regime takes place for large Reynolds numbers, for instance $Re_{StAsym} = 800$ and $Re_{StAsym} = 404$ for $\kappa_i = 0.657$ and $\kappa_i = 2$, respectively^{41,48}.

This brief overview has pointed out that the aspect ratio may affect both features and occurrence of the regimes, with a behavior that sometime is hard to predict as for instance because of the presence of hysteresis. Similarly, other geometrical modifications, such as the inclination of lateral walls of the channels may affect strongly the flow regimes^{14,15}. This may be of importance especially when considering different micro-fabrication techniques, such as laser machining or chemical etching, which may lead to lateral walls which are not perpendicular to the mixer base. The inclination of lateral walls was observed to hamper the symmetry breaking leading to the engulfment regime; however, at low Re numbers mixing is improved because the vortical structures in the mixing channels have different strengths, and thus exhibit a lower degree of symmetry with respect to the vortex regime in case of perpendicular lateral walls¹⁴.

Stability analysis of the flow in T-mixers

Stability analysis provides tools for quantifying important properties of an identified instability which cannot be derived in practice by numerical simulation. While a direct stability analysis allows the identification of a given instability, adjoint methods can be successively employed to provide further information which may be used for a deep characterization of the instability itself and for its control. In this section, after having concisely illustrated the

methodology for stability and sensitivity analysis, we present the results specifically obtained for T-mixers, with focus on the instabilities leading from the vortex to the engulfment regime and to the successive unsteady asymmetric flow regime.

Stability and sensitivity analysis: methodology

Stability analysis is applied to predict whether or not the flow departs from a given state, denoted as the baseflow; in case it does, the baseflow is defined as unstable. In the case of an unstable baseflow, the analysis also provides the path that the flow initially follows as it departs from the unstable configuration. In the results described later in this section the focus is on steady-in-time baseflows, which are thus steady solutions of the Navier-Stokes equations. Moreover, all the analyses described here are linear, i.e., only small amplitude disturbances, ideally infinitesimal ones, are considered. In this specific case the dynamics of the disturbances is described by the Navier-Stokes equations linearized around the baseflow, complemented by homogeneous boundary conditions. Linear stability of the baseflow is thus determined by analyzing the asymptotic-in-time evolution of a generic disturbance. Since the equations are linear, it is possible to use the superposition principle; moreover, the baseflows considered here are fully three-dimensional and without homogeneous directions (i.e., directions along which the baseflow is invariant). In this case a generic disturbance can be searched in the following modal form:

$$\mathbf{v}(\mathbf{x}, t) = \hat{\mathbf{v}}(\mathbf{x}) e^{\lambda t}, \quad (3a)$$

$$p(\mathbf{x}, t) = \hat{p}(\mathbf{x}) e^{\lambda t}, \quad (3b)$$

where both the modal fields ($\hat{\mathbf{v}}(\mathbf{x})$ and $\hat{p}(\mathbf{x})$) and the associated eigenvalue λ are in general complex-valued, implicitly assuming that their real part is taken as the disturbance in physical space. When the modal form (3) is substituted into the linearised Navier-Stokes equations, along with homogeneous boundary conditions, these become an eigenfunction

problem with λ as the associated eigenvalue. The resulting problem, when discretized by a generic numerical method, leads to a discrete generalized eigenvalue problem of the following form:

$$[\mathbf{A}] \{\mathbf{y}\} = \lambda [\mathbf{B}] \{\mathbf{y}\} \quad (4)$$

where the vector $\{\mathbf{y}\}$ collects the discrete eigenfunction (velocity components and pressure), $[\mathbf{A}]$ and $[\mathbf{B}]$ are square and generally sparse matrices of size N_g , N_g being the number of degrees of freedom of the discrete problem, which is typically very large for 3D problems as those at issue here. Therefore, usually dedicated numerical techniques are used in order to explore the spectrum of eq. (4) only in the region of interest in the complex plane (see Camarri⁵⁰ for a review).

If a value of $\lambda = \lambda_r + i\lambda_i$ (λ_r and λ_i being the real and imaginary parts of λ , respectively) exist such that $\lambda_r > 0$, the baseflow is linearly unstable and the associated eigenvector numerically approximates the unstable mode by which the baseflow gets unstable and departs from its configuration. Moreover, if $\lambda_i \neq 0$, the mode initially has an oscillatory-in-time behavior while its amplitude varies in time as $e^{\lambda_r t}$, the period τ of the oscillations being equal to $\tau = 2\pi/\lambda_i$. Conversely, if $\lambda_i = 0$, the mode only grows exponentially in time without oscillations. The resulting flow field is given by the sum of the baseflow and of the eigenmode, whose amplitude and phase is given in time by the complex exponential $e^{\lambda t}$.

Let us now consider the sensitivity problem, i.e., how an identified instability is affected by a perturbation of the flow problem. Focusing for simplicity only on the discrete direct stability problem (4), any perturbation of the system matrix $[\mathbf{A}]$, $[\delta\mathbf{A}]$, which can be induced by a modification of the flow, leads to a perturbation of a given eigenvalue λ , $\delta\lambda$, that can be quantified as follows:

$$\delta\lambda = \frac{\{\mathbf{y}^+\}^H [\delta\mathbf{A}] \{\mathbf{y}\}}{\{\mathbf{y}^+\}^H [\mathbf{B}] \{\mathbf{y}\}} \quad (5)$$

where the superscript H stands for Hermitian and $\{\mathbf{y}^+\}$ is the adjoint eigenvector, defined

as the solution of the following adjoint stability problem:

$$[\mathbf{A}]^H \{\mathbf{y}^+\} = \lambda^* [\mathbf{B}]^H \{\mathbf{y}^+\} \quad (6)$$

where the superscript $*$ stands for complex-conjugate. The result in eq. (5) holds for a generic perturbation $[\delta\mathbf{A}]$. When the objective of the analysis is to explore particular properties of an identified instability, a particular form of $[\delta\mathbf{A}]$ can be selected and substituted in eq. (5). For instance, the core of the instability, i.e., the region in space where the self-sustained mechanism of the global instability acts, can be identified for a particular velocity-force feedback acting only on the linearised stability equations and leading to $[\delta\mathbf{A}] = k [\mathbf{I}_v]$, where $[\mathbf{I}_v]$ is the identity matrix for the velocity components of $\{\mathbf{y}\}$ (in Galerkin methods $[\mathbf{I}_v]$ is the mass matrix for the velocity field) and k is a generic feedback constant. Consequently, eq. (6) shows that the core can be identified as the region where the velocity field of both the direct and the adjoint eigenmodes, properly normalised, are non-negligible at the same time. A scalar quantity can be defined to this purpose, $I = \|\{\mathbf{y}^+\}\| \|\{\mathbf{y}\}\|$, such that the core is localized in regions where I is non negligible.

For control purposes, with focus on passive controls, the variation $[\delta\mathbf{A}]$ can be induced by a proper modification of the baseflow so as to obtain desired stability properties of the modified system. The modification generally depends on a set of control parameters, $\{c_j, j = 1, \dots, N_c\}$. In the case of a perturbation of the baseflow equations, however, the quantification of the matrix perturbation $[\delta\mathbf{A}]$ to be introduced in eq. (5) is not straightforward and can be obtained through an additional forced adjoint problem whose solution is denoted as the adjoint baseflow field $\{\mathbf{y}_b^+\}$. However, once the field $\{\mathbf{y}_b^+\}$ has been computed at the computational cost of solving a linear sparse system of size N_g , $[\delta\mathbf{A}]$ can be successively quantified for a generic combination of the control parameters at the cost of a matrix multiplication, i.e., computationally negligible. Successively $[\delta\mathbf{A}]$ can be plugged in eq. (5) so as to derive the effect of the control on the considered instability by quantifying

the shift $\delta\lambda$ induced on the instability eigenvalue. If, for instance, the objective is to stabilize the flow, then the control is aimed at decreasing the real part of λ , i.e., at shifting the unstable eigenvalue towards the stable region of the complex plane. The advantage of using adjoint methods is that the computational cost for estimating the control effects on the instability is independent of the number of control parameters, N_c , which can be thus very large. Consequently, it is feasible to consider and design distributed controls which are characterized by values of N_c of the same order as N_g . Although these are idealized controls, this kind of analysis can provide quantitative indications on how to design a real flow control. As an example, a locally distributed transpiration of flow through a mixer surface can be imagined as a control; once an optimal distribution of transpiration is found by the adjoint method described above, it is possible to interpret the transpiration as a modification of the geometry which approximates the identified ideal control. This is only one example of how distributed controls can be used to design a real control strategy which can be applied in practice. For more details on the methods mentioned here and on the related numerical aspects we refer to dedicated review papers^{50–52}.

Results for T-mixers

Stability and sensitivity analysis has been applied in the literature to a wide range of flow problems (see again the review papers^{50–52}). Specific applications to T-mixers in order to characterize the instabilities leading to the engulfment and to the unsteady asymmetric regimes are documented in Fani et al.³¹ and Fani et al.⁴² respectively. Examples of application to other similar configurations can be found in Refs.^{53–55}. In the following we will then concisely describe the main results obtained in Fani et al.^{31,42} for a mixer with aspect ratios equal to $\kappa_i = 0.75$ and $\kappa_o = 2\kappa_i = 1.50$ for the inlet and outlet channels, respectively. Although the quantitative results reported thus refer to the particular geometry considered, they qualitatively apply to a large range of geometries and operative conditions as demonstrated in the literature (see the previous section on the effects of the aspect ratio).

Engulfment regime

The instability leading to the engulfment regime is a supercritical pitchfork bifurcation which leads the flow from a symmetric steady regime to an asymmetric steady one. In particular, the flow before the bifurcation has the same two reflectional symmetries of the geometry (and of the incoming flow) while in the postcritical regime both symmetries are broken and the final state has a double-reflection symmetry, i.e., it is invariant for a rotation of π radians around the symmetry axis of the mixing channel. Consequently, the unstable eigenmode of the instability is antisymmetric respect to both the symmetry planes of the geometry. This mode has been computed and characterized from the stability viewpoint for the first time in Fani et al.³¹ for a T-mixer showing a critical Reynolds number for the instability equal to $Re_{StAsym} \simeq 140$. The unstable mode is shown in Fig. 6, where the velocity fields at four representative sections along the outlet channel are considered, confirming the symmetries highlighted above.

For further characterizing the instability, Fani et al.³¹ also computed the corresponding adjoint eigenmode, which is mainly developed in the confluence region and in the inlet channels because convection is partially reversed in the adjoint problem. As a consequence, the overlapping region with the direct mode, which is mainly concentrated at the confluence and in the mixing channel, is very localized in space. In order to have a qualitative picture of the spatial distribution of the direct and adjoint eigenmodes, we report in Fig. 7(a) the vortical structures computed on the direct eigenmode and in Fig. 7(b) an isosurface of the modulus of the adjoint velocity field containing the volume in space where this is non negligible.

Figure 7 indicates that the overlapping region, which corresponds to the instability core, is localized in space at the confluence region of the channels, and it is quantitatively identified in Fig. 8 using isosurfaces of the scalar quantity I previously defined. As shown in the referenced figure, the core of the instability just comprises the separation region which forms on the top wall of the mixer at the confluence of the two opposing streams coming

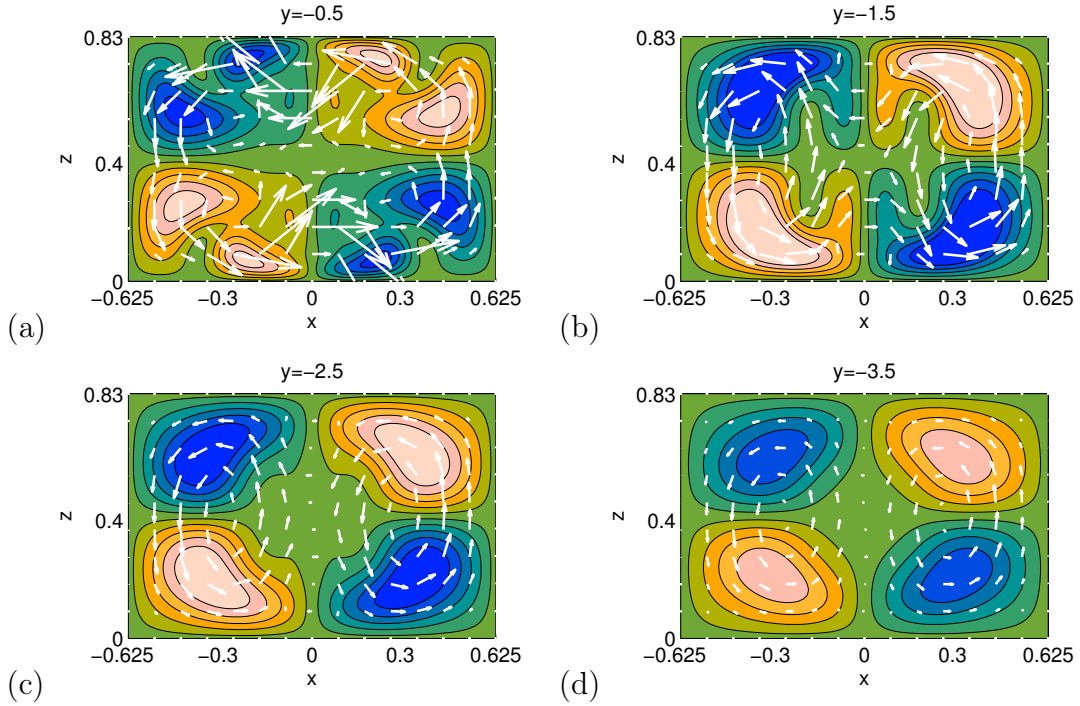


Figure 6: Global direct mode at four different y sections in the mixing channel: (a) $y = -0.5$, (b) $y = -1.5$, (c) $y = -2.5$ and (d) $y = -3.5$, the absolute value of the coordinate y being here the distance of the section from the beginning of the mixing channel. Arrows indicate the in-plane velocity components, whose maximum magnitude is approximately equal to 0.72, and contours represent the velocity component normal to the plane, ranging from -0.6 (dark colour) to 0.6 (light colour). Reprinted with permission from Fani et al.³¹. Copyright 2013 AIP Publishing LLC.

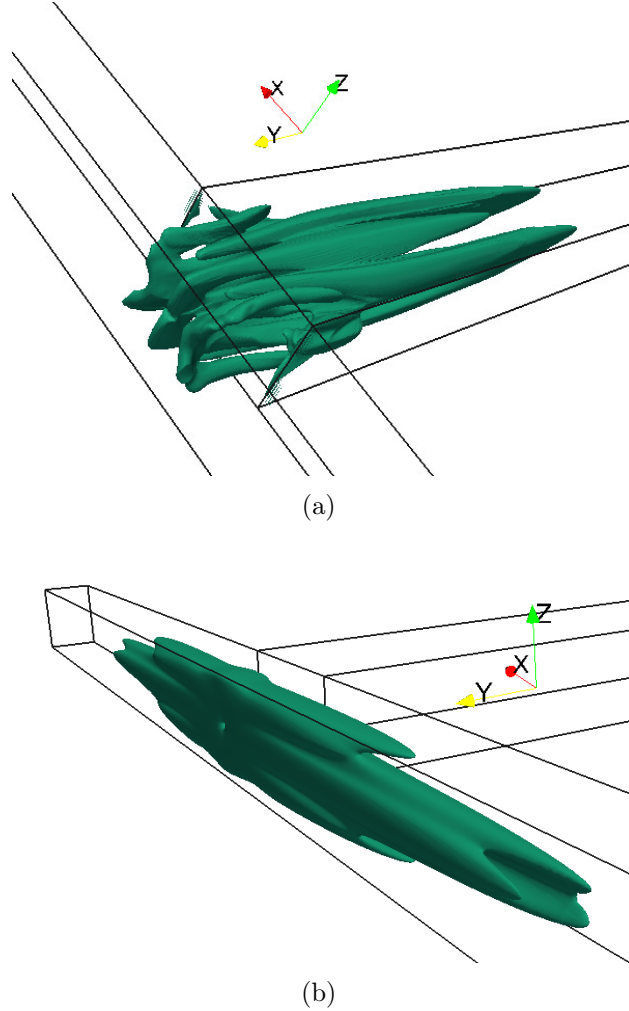
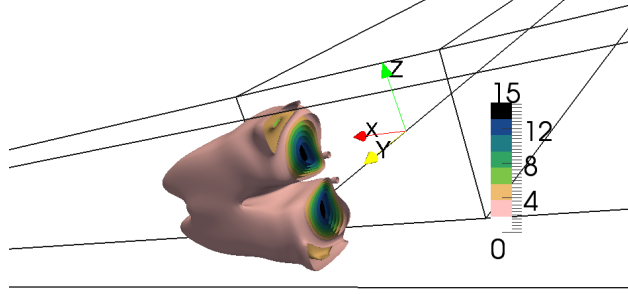
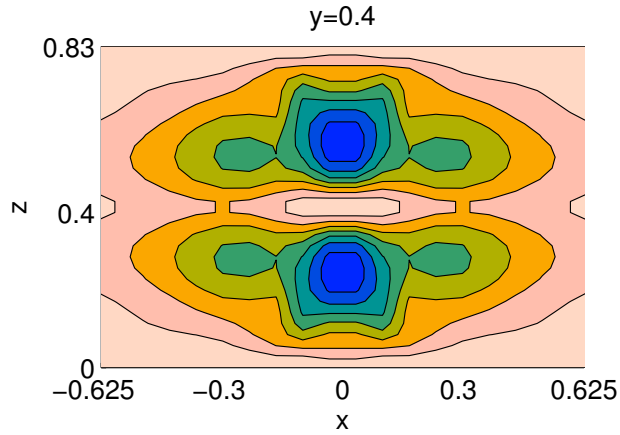


Figure 7: Engulfment instability: (a) vortical structures identified by the λ_2 criterion, computed on the direct eigenmode and (b) modulus of the adjoint velocity field containing the volume where this is non negligible. Adapted with permission from Fani et al.³¹. Copyright 2013 AIP Publishing LLC.

from the inlet channels. This is the same region where the crucial effect of the engulfment regime takes origin, i.e., the tilting of the separation region which leads to the asymmetric distribution of vorticity inside the four vortices forming in that separation region and being convected into the mixing channel (see also the description in the previous section on the flow regimes). It is the asymmetric intensity of such vortices in the mixing channel which promotes mixing through convection and differentiate the engulfment from the vortex regime, where the vortices are indeed symmetric. Thus, the sensitivity analysis in Fani et



(a)



(b)

Figure 8: Instability core $\|\hat{\mathbf{u}}\|\|\mathbf{u}^+\|$, computed at $Re = 140$. (a) 3D view and (b) slice at $y = 0.4$, i.e., inside the inlet channels at a distance equal to 0.4 from the beginning of mixing channel. Reprinted with permission from Fani et al.³¹. Copyright 2013 AIP Publishing LLC.

al.³¹ demonstrates that the instability takes origin in a very localized region of the flow field, and that an effective control of the instability can be obtained only acting so as to modify the flow in that specific region.

As concerns the control of the engulfment instability, in Fani et al.³¹ control maps were also derived by adjoint methods showing the effect of a distributed transpiration velocity on the mixer wall; they are reported here in Fig. 9(a) and Fig. 9(b) for the top and lateral walls. The proposed control maps allow to quantify the modification of the unstable eigenvalue for generic distributions of transpiration by simply computing surface integrals. As an example, suppose that we want to evaluate the effect $\delta\lambda$ on the instability eigenvalue λ induced by

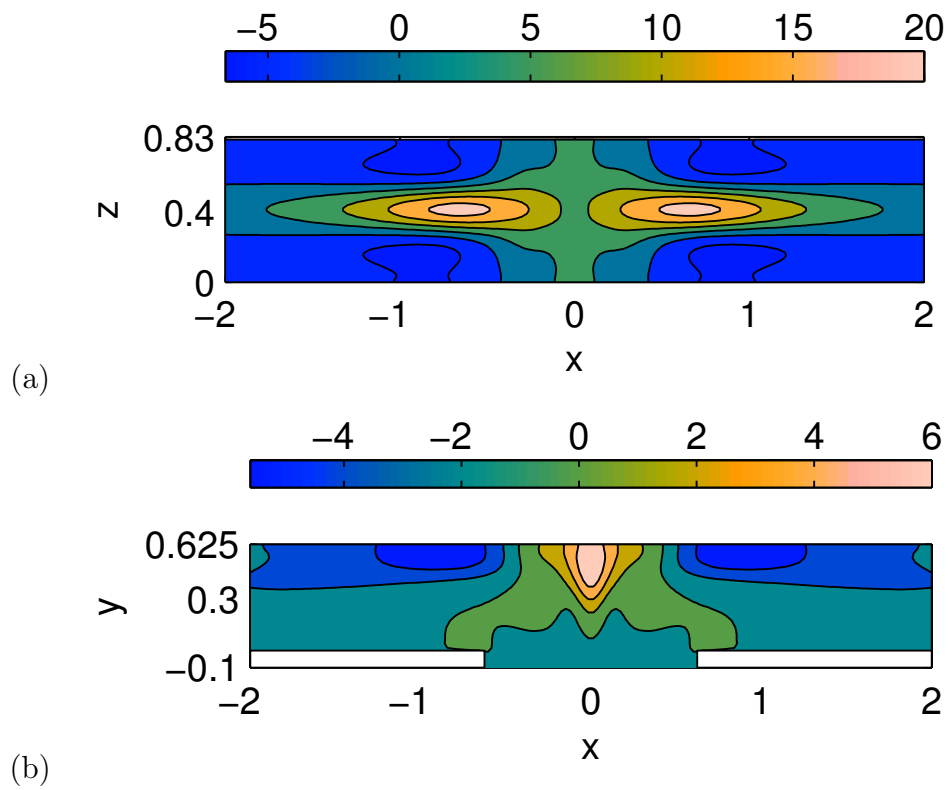


Figure 9: Control maps: sensitivity to the introduction of a velocity profile normal to wall; (a) top and (b) side walls of the T-mixer. Reprinted with permission from Fani et al.³¹. Copyright 2013 AIP Publishing LLC.

a distributed velocity transpiration $v_n(\mathbf{x})$ acting on the top wall of the mixer. We remind that λ and $\delta\lambda$ are real-valued for the considered instability. In this case, denoting as $m(\mathbf{x})$ the map in Fig. 9(a) and with S_t the top wall, $\delta\lambda$ is (linearly) quantitatively estimated as follows:

$$\delta\lambda = \iint_{S_t} m(\mathbf{x}) v_n(\mathbf{x}) dS(\mathbf{x}) . \quad (7)$$

In particular, a jet which implies a negative wall-normal velocity with respect to the normal direction pointing outside the flow domain has a stabilizing effect (i.e., $\delta\lambda < 0$) if placed in regions of the top wall where the map in Fig. 9(a) is positive. If we interpret it as a tilting angle imposed to the top wall, this implies that imposing an angle to the incoming channel of the mixer does have an effect on the onset of the engulfment regime, as will be discussed in more details in the next section. In particular, when the flows from the inlet channels have a positive component in the direction of the outlet one (Y-mixers) the value of Re_{StAsym} increases while in the opposite case (arrow-mixers) Re_{StAsym} decreases. This is confirmed by numerical simulations and experiments, as commented in more details in the following sections.

The same strategy used to derive the maps in Fig. 9 has been used in Fani et al.³¹ to quantify the effect of a variation in the velocity distribution at the inlet boundaries of the mixer on the instability. The corresponding map, which is validated by the numerical simulations in³¹, is reported in Fig. 10. The map shows that a decrease of the inflow velocity at a generic location of the inflow section always implies a negative shift of the eigenvalue, and thus a delay of the engulfment in terms of flow Reynolds numbers. However, the map in Fig. 10 also shows that the stabilizing or destabilizing effect depends on the location of the velocity perturbation and that the sensitivity is not symmetric respect to the symmetry plane for the geometry.

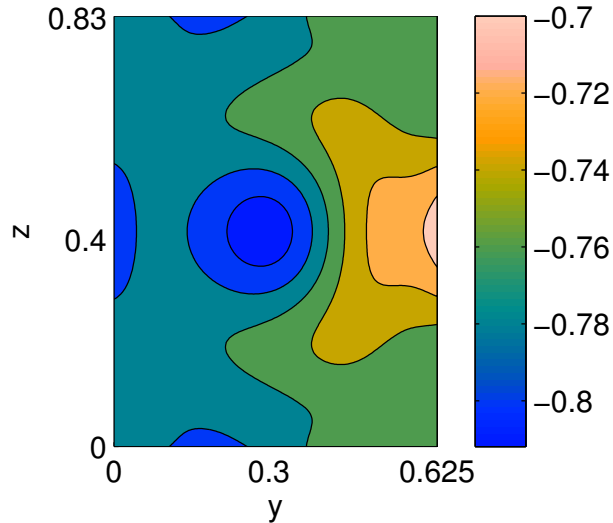


Figure 10: Control map: sensitivity to modifications of the velocity profile normal to the inlet plane. Adapted with permission from Fani et al.³¹. Copyright 2013 AIP Publishing LLC.

Unsteady asymmetric regime

If the Reynolds number is increased beyond a second critical value, Re_{cr2} , the flow leaves the engulfment regime and becomes time periodic; moreover, the time-averaged flow field does not respect the same symmetries of the geometry. Due to these characteristics, the new flow regime observed when $Re > Re_{UnstAsym}$ is denoted as the Unsteady Asymmetric Regime (UAR, see the previous section on flow regimes). The onset of the UAR has been studied by a dedicated stability analysis in Fani et al.⁴². In this case the bifurcation leading the flow to the UAR is a supercritical Hopf bifurcation, and the couple of complex-conjugate eigenvalues associated with this instability have been identified by studying the stability of the flow, when this is in the engulfment regime, as a function of the flow Reynolds number. In the particular geometry considered in Fani et al.⁴² the onset of the UAR is observed in the range $220 \leq Re_{UnstAsym} \leq 230$. As for the engulfment instability, the instability leading to the UAR has been characterized by computing the direct and adjoint eigenmodes, whose spatial distribution is shown in Fig. 11. The figure shows that also in this case the direct and adjoint modes have different spatial distribution and that the overlapping region between

the two is again localized at the confluence region between the three channels. This aspect

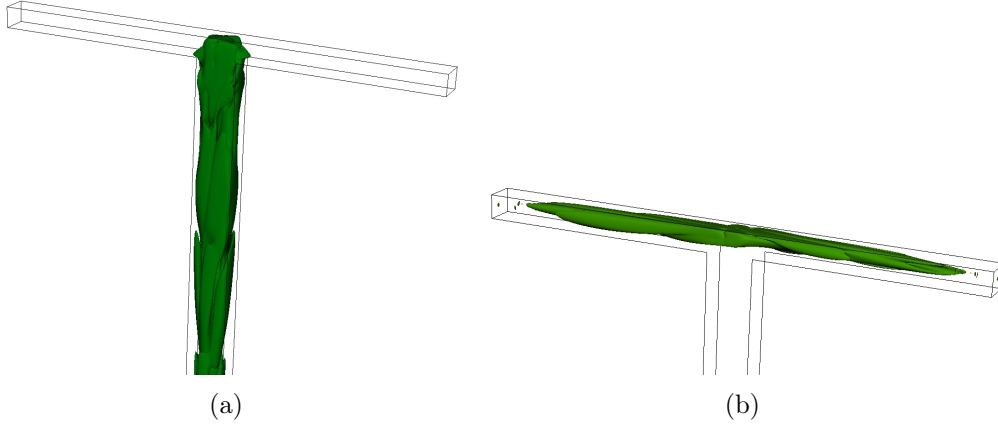


Figure 11: Global (a) and adjoint (b) eigenmodes for the UAR, depicted by an isosurface at a small threshold value of the magnitude of the real part of the velocity field, computed at $Re = 220$. Adapted with permission from Fani et al.⁴². Copyright 2014 AIP Publishing LLC.

is highlighted in Fig. 12, where the core of the instability is reported, showing that also in this case the crucial role for the onset of the instability is played by the separation region forming on the top wall of the mixer, as for the engulfment instability. This is confirmed by the simulations reported in Fani et al.⁴² and in Mariotti et al.^{33,46}, which show that the flow dynamics in a time period τ is completely determined by the evolution of the vortical structures originating and periodically evolving in the separation region. The overall flow dynamics is then determined by such vortical structures as they are successively convected into the mixing channel.

As the UAR instability is an Hopf bifurcation, the associated eigenvalue λ found by stability analysis in Fani et al.⁴² is complex valued. Consequently, the control maps derived by sensitivity analysis are also complex valued in this case, and their real and imaginary parts correspond to the control maps for the real and imaginary parts of λ , respectively, as the control applied in physical space is real-valued. We remind that controlling λ_r is equivalent to control the temporal growth rate of the instability, while changing λ_i leads to a variation of the period of oscillation of the instability. With this premise, the application of the control maps is identical to eq. (7). An example of control maps for a generic variation

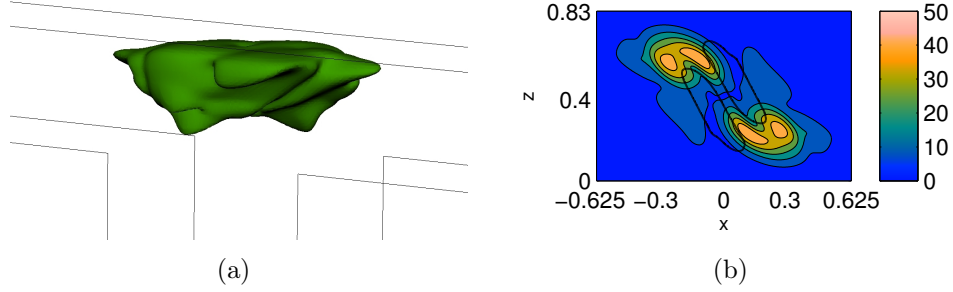


Figure 12: Instability core $\|\mathbf{u}^+\| \|\hat{\mathbf{u}}\|$ at $Re = 220$. (a) Three dimensional view and (b) slice at $y = 0.5$, i.e., in the inlet channels at a distance equal to 0.5 from the beginning of the mixing channel. The base-flow vortices in (b) are identified (tick line) by using the λ_2 criterion. Reprinted with permission from Fani et al.⁴². Copyright 2014 AIP Publishing LLC.

of the inlet velocity profile for the UAR instability is reported in Fig. 13. The frequency sensitivity in Fig. 13 refers to the quantity $\delta\lambda_i/2\pi$. The maps at the first inlet, plotted in Fig. 13(a) and Fig. 13(c), can be obtained from those referring to second inlet ones, i.e. those in Fig. 13(b) and Fig. 13(d), through a reflection around the plane $z = H/2$. It is interesting to note that the sign of the growth factor sensitivity in Fig. 13(a) and (b) is always negative. This implies that decreasing the inflow velocity, even if locally, always implies a negative shift of the eigenvalue $\delta\lambda_r < 0$, i.e., a stabilizing effect. However, the sensitivity is not uniform and regions of higher sensitivity exists. Moreover, it is possible to perturb the inflow profile so as to preserve the mass flow rate but to have an effect on the instability growth rate at the same time. As concerns the frequency of the eigenmode, Figs. 13(c) and 13(d) show that a localized decrease (increase) of the inflow velocity at a generic location of both inflow boundaries always leads to a decrease (increase) of the instability frequency. This is consistent with the simulations in Fani et al.⁴² showing that the frequency of the instability increases as Re is increased.

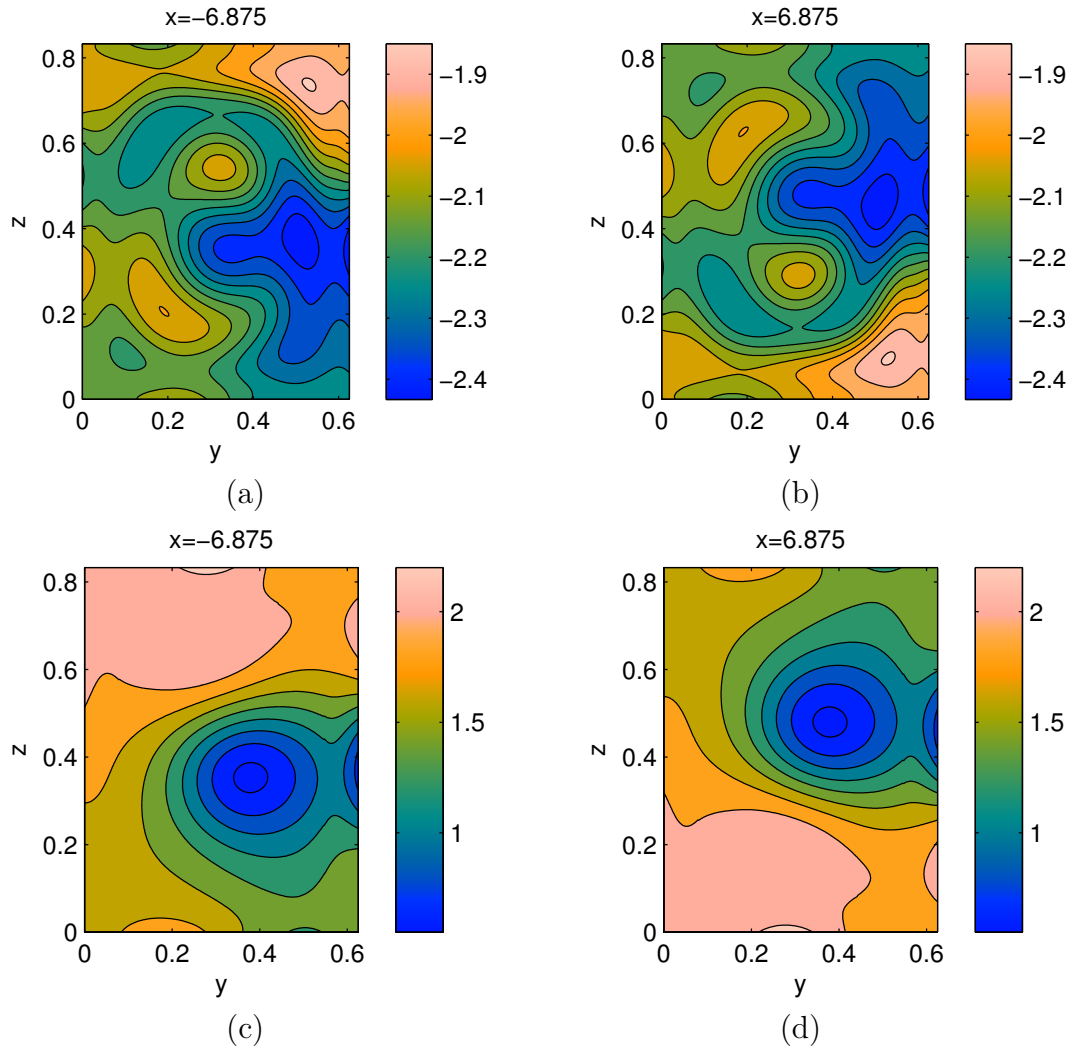


Figure 13: Sensitivity to modifications of the velocity profile normal to the inlet plane for the UAR instability at $Re = 220$, computed at the two inlet surfaces (i.e., $x = \pm 6.875$). Growth rate (a)(b) and frequency (c)(d) sensitivities. Reprinted with permission from Fani et al.⁴². Copyright 2014 AIP Publishing LLC.

Arrow-mixers

Engulfment regime

The sensitivity analysis described in the previous section pointed out that the core of the instability leading to the engulfment regime, i.e., the region where this instability originates, is located near the top mixer wall at the confluence of the two streams. This suggests that a possible way to promote the onset of the engulfment is to introduce geometrical modifications, also small, in that region. One simple geometrical modification consists in varying the angle between the axes of the inlet channels and that of the mixing channel. We focus herein on arrow-mixers, obtained by tilting downward the axes of the inlet channels (see the sketch in Fig. 14). As it will be described more in detail in the following, this type of configuration is interesting because it is characterized by critical Reynolds numbers for the onset of the engulfment regime lower than for T-mixers.

A first numerical investigation was carried out by Soleymani et al.⁴⁸ for mixers having square inlet cross-sections, i.e., with $\kappa_i = 1$ and different angles between the inlet channel axes; a fixed Reynolds number was considered which for the T-mixer was in the engulfment regime. It was observed that the mixing efficiency was maximum for the arrow-mixer having a mixing angle, i.e the angle between the inlet channel axes, $\theta = 210^\circ$. Siconolfi et al.⁵⁶ computed through numerical simulations and stability analysis the critical Reynolds numbers for the onset of the engulfment regime for different arrow-mixers. The aspect ratios of the channels in Siconolfi et al.⁵⁶ are the same as those of the mixer described in the previous section i.e., $\kappa_i = 0.75$ and $\kappa_o = 2\kappa_i = 1.50$; the methodology used for the stability analysis is also the same as the one previously described. The onset of the engulfment regime was found to occur at lower Reynolds numbers for arrow-shaped mixers. The reduction of the critical Reynolds number for the engulfment onset was found to monotonically increase with the mixing angle. For instance, for a mixing angle of $\theta = 220^\circ$ the engulfment regime was found to occur at $Re \simeq 100$ and for $\theta = 200^\circ$ at $Re \simeq 110$, while the critical Reynolds

number for the T-mixer having the same aspect ratios was about 140. We refer to Siconolfi et al.⁵⁶ for more details. These findings were confirmed by more recent numerical⁵⁷ and joint experimental and numerical^{58,59} investigations. Therefore, arrow-mixers are interesting from a practical view point because they trigger mixing at lower Re compared to T-mixers and this effect is more pronounced as the mixing angle increases.

However, Galletti et al.⁶⁰ first observed a non-monotonic behavior of mixing with increasing Reynolds number in the engulfment regime in numerical simulations of an arrow-mixer with $\theta = 220^\circ$ and square inlet cross-sections. They suggested that the reduction of the mixing degree can be ascribed to the formation of a strong vortical structure and of a high velocity region at the center of the mixing channel. This observation motivated the systematic study carried by means of numerical simulations and experimental flow visualizations by Mariotti et al.⁵⁹. Mixer configurations having square inlet cross-sections and mixing angles $\theta = 180^\circ$ (T-mixer), 200° , 210° , 220° and 230° were considered. Figure 15 summarizes the results obtained by Mariotti et al.⁵⁹ in terms of mixing degree as a function of the Reynolds number, based on the inlet bulk velocity and on the hydraulic diameter of the mixing channel. The tilting angle, α , in Fig. 15 is the angle between the axes of the inlet channels and the direction normal to the mixing channel axis, positive downstream (see also Fig. 14). We refer once again to Mariotti et al.⁵⁹ for the precise definition of δ_m . Figure 15 clearly shows that, as previously discussed, by increasing the tilting angle the Reynolds number at which the mixing suddenly increases, due to the onset of the engulfment regime, monotonically decreases. However, it can be noticed that the arrow-mixers with the smallest tilting angles are characterized by a monotonic increase of δ_m with Re within the engulfment regime, as it happens for T-mixers, but this is not the case for arrow-mixers having $\alpha \geq 20^\circ$ ($\theta \geq 220^\circ$). Indeed, for these mixers, after a first increase when entering in the engulfment regime, δ_m shows a significant drop with Re to eventually increase again. The values of Re at which this drop occurs once again depend on the tilting angle. Mariotti et al.⁵⁹ also showed that the drop in the mixing performance is related with a change in the flow topology; indeed, this

drop occurs when the two top parts of the 3D vortical structure typical of the engulfment regime in T-mixers, previously described, have disappeared and the two corotating legs in the mixing channel have merged in a unique vortical structure, as also observed in Galletti et al.⁶⁰. An example is given in Fig. 16 for $\theta = 220^\circ$. The velocity field induced by the single structure surviving in the mixing channel is less efficient in promoting mixing than those present in the typical engulfment flow, as can also be seen in Fig. 16, and this explains the aforementioned drop of the mixing degree. By further increasing Re , the vortical structure in the mixing channel grows in size and, hence, δ_m starts to increase again. The above described change in flow topology does not occur for T-mixers or for arrow ones with $\theta < 220^\circ$. From a practical viewpoint, it appears thus that for arrow-mixers with large mixing or tilting angles a careful control of the operating conditions is needed in the engulfment regime to maintain an efficient mixing level.

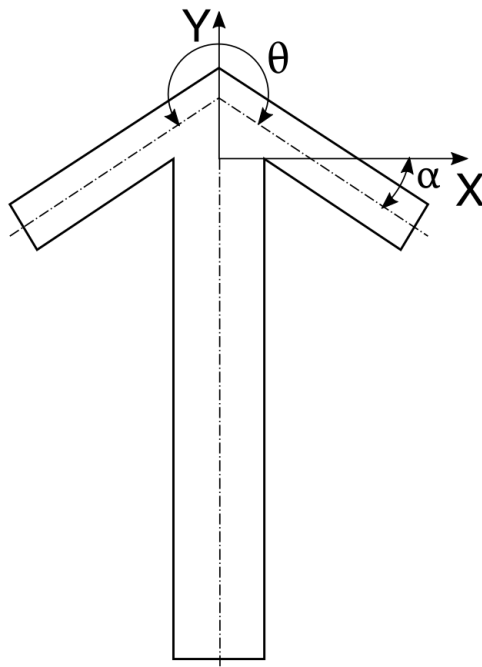


Figure 14: Sketch of an arrow-shaped mixer.

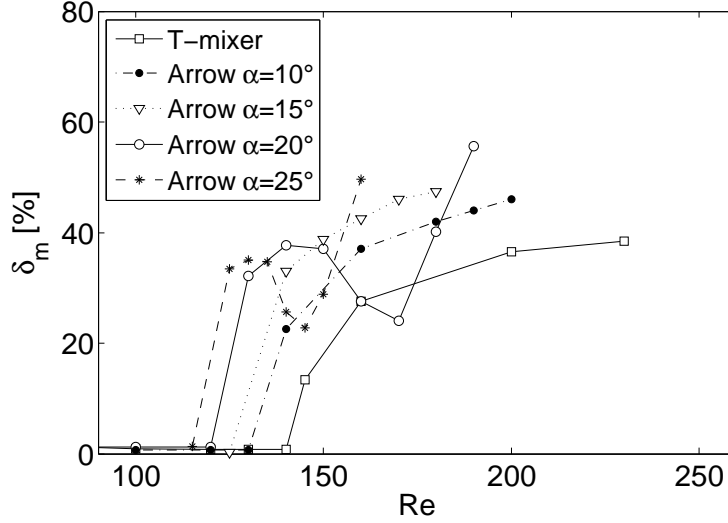


Figure 15: Mixing degree as a function of the Reynolds number for the T-shaped micro-mixer and for arrow-mixers with different angles, from numerical simulations in Mariotti et al.⁵⁹. Reprinted with permission from Mariotti et al.⁵⁹. Copyright 2019 American Physical Society.

Time-periodic regimes

As previously described, in T-mixers unsteady periodic regimes eventually establish by increasing the Reynolds number after the engulfment. The unsteady flow regimes in two arrow-mixers having $\theta = 200^\circ$ and $\theta = 220^\circ$ were recently investigated in Mariotti et al.⁶¹ The inlet channels have again square cross-sections and the analysis was carried out by experimental flow visualizations and numerical simulations. The results are summarized in Fig. 17 in terms of mixing degree vs. Reynolds number. The curve relative to the T-mixer reflects the behavior previously described: monotone increase of mixing in the engulfment regime followed by a further increase in the periodic asymmetric regime and then by a sudden drop with the onset of the periodic symmetric regime. As for the arrow-mixer with the larger mixing angle, the first drop corresponds to the previously discussed change of flow topology, i.e., steady flow with a single vortex in the mixing channel. The first unsteady regime for this arrow-mixer is characterized by the periodic motion of this single vortical structure which leads to an efficient mixing. By further increasing Re , the flow first becomes again steady with a topology similar to that of the vortex regime occurring at much lower

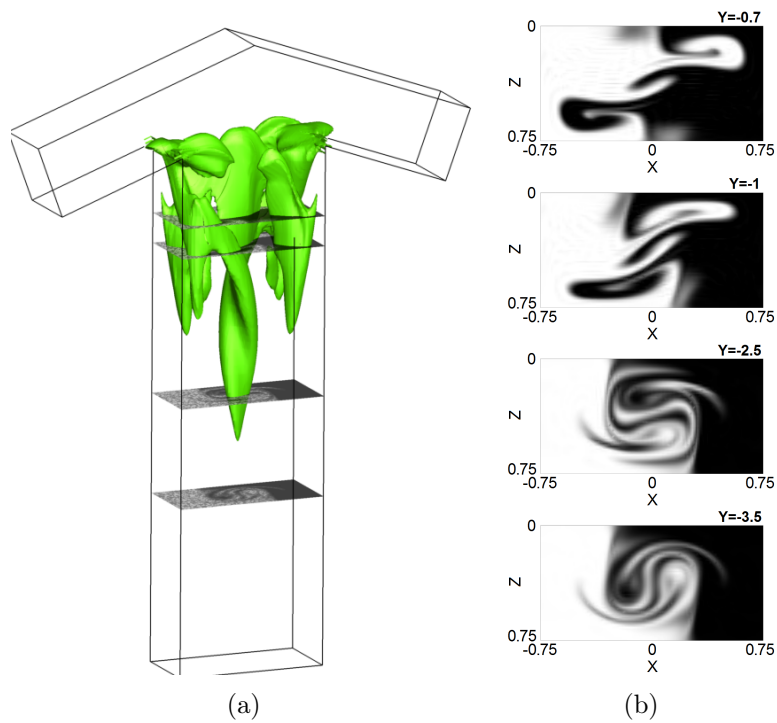


Figure 16: Isosurface of the λ_2 vortex indicator (a) and dye concentration fields (b) at $Re = 170$, from numerical simulations in Mariotti et al.⁵⁹ for a arrow-mixer with $\theta = 220^\circ$. Adapted with permission from Mariotti et al.⁵⁹. Copyright 2019 American Physical Society.

Re , and then unsteady again, characterized by the periodic tilting of the vortical structures near the top walls of the mixer, but by minor variations of the flow features in the mixing channel. In both these conditions the mixing efficiency becomes again very low. Note that the arrow-mixer with $\theta = 220^\circ$ has better efficiency than the T-mixer only in limited ranges of Re , confirming that also for relatively high Reynolds a careful control of operating conditions is needed for this configuration. Conversely, the arrow-mixer with the lowest mixing angle is characterized by values of δ_m globally larger than those of the T-mixer over the whole considered range of Re . By analyzing more in detail the behavior for $\theta = 200^\circ$ ($\alpha = 10^\circ$), the first unsteady regime is very similar to the asymmetric one occurring for T-mixers and this implies a monotone increase of δ_m with Re . Unlike what happens in T-mixers, by further increasing Re , however, the flow dynamics becomes very similar to that of the first unsteady regime in the other arrow-mixer configuration, with a single vortical structure oscillating in the mixing channel. This corresponds to a good mixing efficiency, and thus to a monotonic increase of mixing. All the flow regimes occurring in the considered mixer configurations are summarized in Fig. 18.

Summarizing, the mixing angle, or equivalently the tilting one, in arrow-mixers has a strong impact on the mixing performances also at relatively high values of Re in unsteady periodic regimes and it appears that a small downward tilting angle leads to an improvement of the mixing performances, compared to those of classical T-mixers, which is robust to variations in the operating conditions, up to transition to a chaotic dynamics.

Concluding remarks

As shown in the overview presented herein, micro T-mixers operating with a single fluid are characterized by remarkably varying mixing performances also in laminar conditions (low Reynolds numbers). It has been pointed out how the mixing efficiency is deeply related to the topology and dynamics of the flow, which can be complex in spite of the simple

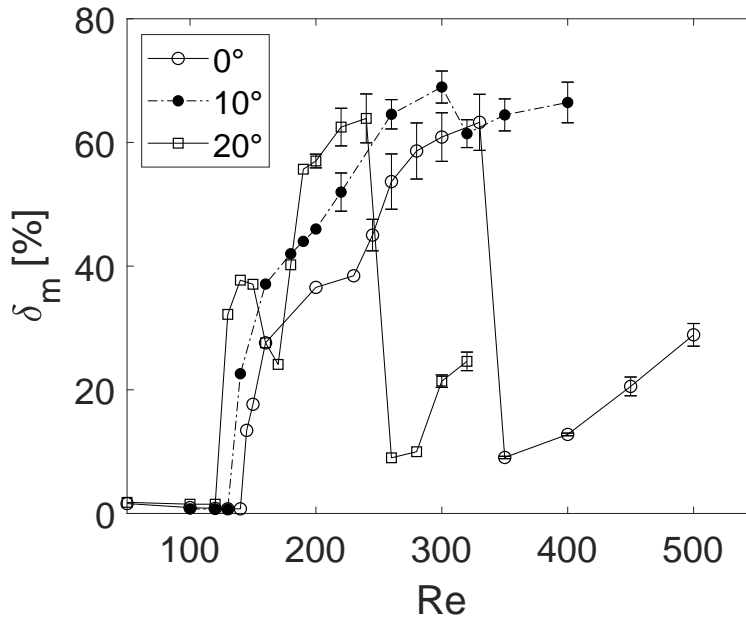


Figure 17: Degree of mixing numerically evaluated at the cross-section $Y = -8$ as a function of the Reynolds number Re and of the tilting angle α from numerical simulations in Mariotti et al.⁶¹.

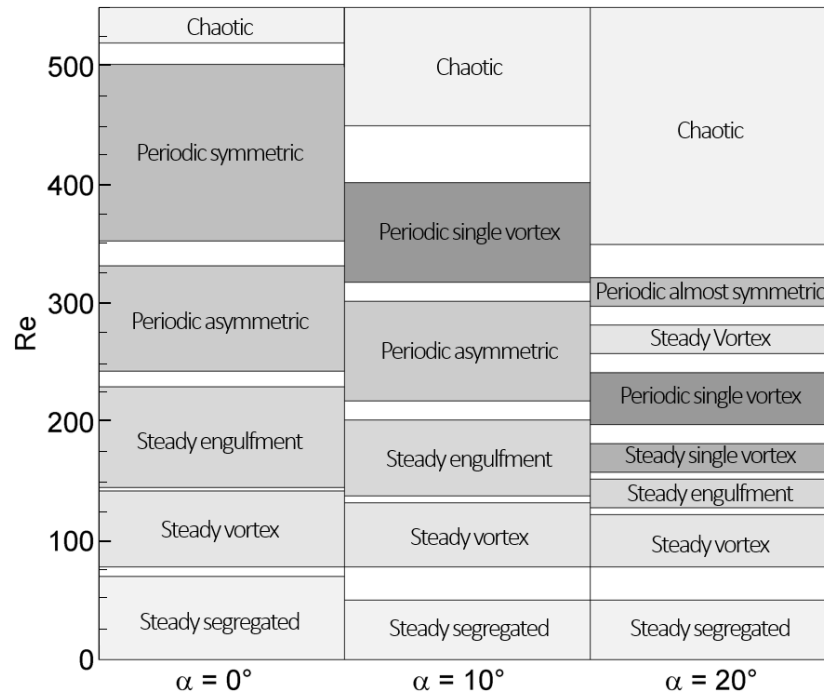


Figure 18: Summary of the flow regimes as a function of the Reynolds number and of the tilting angle α from numerical simulations and experiments in Mariotti et al.⁶¹.

geometry and the absence of turbulence. In particular, except in the segregated regime at very low Reynolds numbers, complex 3D vortical structures characterize the flow. Their loss of symmetry leads to the onset of the engulfment regime, while unsteady regimes are also dominated by the dynamics of these structures.

The key role of 3D vortical structures is also confirmed by three-dimensional linear stability analysis, whose main results are also reviewed herein. This analysis allows the hydrodynamic instabilities leading to the onset of the different flow and mixing regimes to be determined. In all cases, the core of the instability, i.e., the region where the instability originates, is localized around the flow recirculations near the top wall at the confluence of the inlet streams, from which the top parts of the vortical structures originate. By carrying out jointly also a sensitivity analysis, useful information can be obtained on how the flow and, hence, mixing, can be controlled by promoting or preventing the onset of the different regimes. An example of a geometrical change suggested by stability and sensitivity analysis is the downward tilting of the axes of the inlet channels, leading to arrow-shaped mixers. This simple change not only influences the onset of the different flow regimes, but it also leads to flow topologies and dynamics not observed for T-mixers, which once again deeply influence the mixing performances. From a practical viewpoint, it appears that a small downward tilting angle leads to an improvement of the mixing performances, compared to those of classical T-mixers in the whole range of operating conditions (up to transition to turbulence).

Several additional aspects have not been reviewed in detail herein for the sake of brevity and the interested readers are referred to the cited references. For instance, many different and more complex geometrical modifications can be considered as well as changes/perturbations in the inlet conditions. When dealing with micro reactors, two or more fluids having different properties are present and this may affect, both quantitatively and qualitatively, the flow regimes and mixing. This issue has been addressed in the literature and the relevant references have been given in the text; however, there is room for additional investigations.

Finally, when chemical reactions occur, an efficient mixing may be more or less beneficial to obtain a high reaction yield depending on how the reaction characteristic times compare with those of mixing and flow. This issue still needs to be fully understood and characterized to our knowledge. Finally, the precipitation of nanoparticles is a further important application of micro-mixers, not covered here, which is increasingly addressed in the literature by coupling numerical simulation with simple models of precipitation, as e.g. population balance (see e.g. Schikarski et al.⁶² and Gradl et al.⁶³ and the references therein).

Appendix. Computational limit: small and large scales

In most of the previous works on liquid mixing, it has been stressed that, as the Schmidt number in liquid mixture is very large, the composition field varies over distances that are much smaller than those related to the velocity field. In fact, defining the Batchelor number, Ba , as the ratio between the smallest lengthscale of the composition field and that of the velocity field (e.g., the Kolmogorov lengthscale in the case of turbulent flow), it is expected that $Ba = 1/\sqrt{Sc}$ (see Batchelor⁶⁴, Ottino⁶⁵ and Bothe et al.⁶⁶). Naturally, considering that, for a typical low viscosity liquid mixture, $Sc \approx 10^4$, we see that the mesh size that is required to resolve the composition field is unacceptably small, and therefore some clever numerical scheme must be devised to circumvent this problem. For example, simulating the reactive mixing process in the mixing channel of a T-junction, Bothe et al.⁶⁶ applied a hybrid numerical scheme, exploiting the fast redirection of the flow inside the channel. A similar approach was proposed recently to simulate mixing in T-microdevices by Borgogna et al.⁶⁷ and Giona et al.⁶⁸, combining a Monte Carlo method near the confluence region, with the exact solution of material transport in the mixing channel, where the flow is almost one-dimensional.

In reality, as noted by Hinch⁶⁹ (see Section 3.5) using scaling arguments, in the presence of straining motion there is fortunately a faster mechanism of mixing, due to the flow-induced

exponential increase of the interfacial area between unmixed regions. Similarly, in the case of laminar mixing in the confluence region of a T-mixer, Ottino and Wiggins⁷⁰ showed that the typical lengthscale of the velocity field and that of the composition field are of the same order of magnitude. This prediction was confirmed in a recent work by Galletti et al.¹⁶, who showed that for Reynolds numbers $Re = 100$ and 150 , simulation results are independent of the Schmidt number, provided that $Sc > 10^3$, which effectively corresponds to the passive tracer limit. This results agree with Orsi et al.¹⁸, who applied the homogenization multiple-scale technique to show that, at leading order, when the fluid velocity is not perpendicular to the material flux, molecular diffusivity can be neglected altogether. Therefore, in simulating the mixing process of two identical fluids in a T-junction, at the confluence region the fluid flow is quite complex, ensuring that at leading order, when $Sc \gg 1$, molecular diffusion does not play any role. On the other hand, in the mixing channel, when there is almost no transverse flow, this approximation is not valid and one of the previously mentioned numerical scheme must be applied to resolve the small length scales associated with the concentration field. Naturally, when the two liquids have different viscosities and, upon mixing, form a mixture with a composition-dependent viscosity, even if initially the two species move in a segregate regime, i.e., parallel to each other, they will develop a transversal velocity, proportional to the viscosity gradient, thus inducing a transversal convective mass flux which, at large Sc , will smoothen the composition field, even in the absence of molecular diffusion.

References

- (1) Löb, P.; Löwe, H.; Hessel, V. Fluorinations, chlorinations and brominations of organic compounds in micro reactors. *J. Fluorine Chem.* **2004**, *125*, 1677.
- (2) Löbbbecke, S.; Antes, J.; Ferstl, W.; Boskovic, D.; Türcke, T.; Schwarzer, M.; Krause, H. Microreactors for Processing of Hazardous and Explosible Reactions. IChemE Symposium Series No. 153: Proceed. 12th International Symposium Loss Prevention and Safety Promotion in the Process Industries, Edinburgh, UK, 22. 2007.
- (3) Roberge, D. M.; Ducry, L.; Bieler, N.; Cretton, P.; Zimmermann, B. Microreactor Technology: A Revolution for the Fine Chemical and Pharmaceutical Industries? *Chem. Eng. Technol.* **2005**, *28*, 318.
- (4) Zhao, C.-X.; He, L.; Qiao, S.; Middelberg, A. Nanoparticle synthesis in microreactors. *Chem. Eng. Sci.* **2011**, *66*, 1463.
- (5) Shi, H.; Nie, K.; Dong, B.; Long, M.; Xu, H.; Liu, Z. Recent progress of microfluidic reactors for biomedical applications. *Chem. Eng. J.* **2019**, 635.
- (6) Kumar, V.; Paraschivoiu, M.; Nigam, K. D. P. Single-phase fluid flow and mixing in microchannels. *Chem. Eng. Sci.* **2011**, *66*, 1329.
- (7) Hessel, V.; Löwe, H.; Schönfeld, F. Micromixers-a review on passive and active mixing principles. *Chem. Eng. Sci.* **2005**, *60*, 2479.
- (8) Lee, C.-Y.; Wang, W.-T.; Liu, C.-C.; Fu, L.-M. Passive mixers in microfluidic systems: a review. *Chem. Eng. J.* **2016**, *288*, 146.
- (9) Nguyen, N.-T.; Wu, Z. Micromixers - a review. *J. Micromech. Microeng.* **2005**, *15*, R1.
- (10) Roudgar, M.; Brunazzi, E.; Galletti, C.; Mauri, R. Numerical Study of Split T-Micromixers. *Chem. Eng. Technol.* **2012**, *35*, 1291.

- (11) Ansari, M. A.; Kim, K.-Y.; Anwar, K.; Kim, S. M. Vortex micro T-mixer with non-aligned inputs. *Chem. Eng. J.* **2012**, *181*, 846.
- (12) Sultan, M. A.; Fonte, C. P.; Dias, M. M.; Lopes, J. C. B.; Santos, R. J. Experimental study of flow regime and mixing in T-jets mixers. *Chem. Eng. Sci.* **2012**, *73*, 388.
- (13) Santos, R. J.; Sultan, M. A. State of the Art of Mini/Micro Jet Reactors. *Chem. Eng. Technol.* **2013**, *36(6)*, 937.
- (14) Mariotti, A.; Lanzetta, M.; Dini, G.; Rossi, A.; Brunazzi, E.; Mauri, R.; Galletti, C. Influence of cross-sectional geometry on mixing in a T-shaped micro-junction. *Chem. Engineer. Trans.* **2019**, *74*, 955.
- (15) Kockmann, M.; Engler, C.; Föll, P.; Woias, P. Liquid mixing in static micro-mixers with various cross sections. Proceedings of the First International Conference on Micro Minichannels, ASME, Rochester, NY. 2003.
- (16) Galletti, C.; Arcolini, G.; Brunazzi, E.; Mauri, R. Mixing of binary fluids with composition-dependent viscosity in a T-shaped micro-device. *Chem. Eng. Sci.* **2015**, *123*, 300.
- (17) Galletti, C.; Brunazzi, E.; Mauri, R. Unsteady mixing of binary liquid mixtures with composition-dependent viscosity. *Chem. Eng. Sci.* **2017**, *164*, 333.
- (18) Orsi, G.; Roudgar, M.; Brunazzi, E.; Galletti, C.; Mauri, R. Water-ethanol mixing in T-shaped microdevices. *Chem. Eng. Sci.* **2013**, *95*, 174.
- (19) Schikarski, T.; Peukert, W.; Avila, M. Direct numerical simulation of water-ethanol flows in a T-mixer. *Chem. Eng. J.* **2017**, *324*, 168.
- (20) Lobasov, A.; Minakov, A. Analyzing mixing quality in a T-shaped micromixer for different fluids properties through numerical simulation. *Chem. Eng. Process.* **2018**, *124*, 11.

- (21) Galletti, C.; Roudgar, M.; Brunazzi, E.; Mauri, R. Effect of inlet conditions on the engulfment pattern in a T-shaped micro-mixer. *Chem. Eng. J.* **2012**, *185-186*, 300.
- (22) Schikarski, T.; Trzenschiok, H.; Peukert, W.; Avila, M. Inflow boundary conditions determine T-mixer efficiency. *Reaction Chemistry and Engineering* **2019**, *4*, 559.
- (23) Kockmann, N.; Föll, C.; Woias, P. Flow regimes and mass transfer characteristics in static micro mixers. *Proceedings of SPIE - The International Society for Optical Engineering* **2003**, *4982*, 319.
- (24) Kockmann, N.; Engler, M.; Woias, P. *Convective mixing and chemical reactions in T-shaped micro reactors*; AIChE Annual Meeting, Conference Proceedings; 2004; p 5973.
- (25) Engler, M.; Kockmann, N.; Kiefer, T.; Woias, P. Numerical and experimental investigations on liquid mixing in static micromixers. *Chem. Eng. J.* **2004**, *101*, 315.
- (26) Wong, S.; Ward, M.; Wharton, C. Micro T-mixer as a rapid mixing micromixer. *Sensors Actuat. B-Chem.* **2004**, *100*, 359.
- (27) Bothe, D.; Stemich, C.; Warnecke, H.-J. In *16th European Symposium on Computer Aided Process Engineering and 9th International Symposium on Process Systems Engineering*; Marquardt, W., Pantelides, C., Eds.; Computer Aided Chemical Engineering; Elsevier, 2006; Vol. 21; p 351.
- (28) Dreher, S.; Kockmann, N.; Woias, P. Characterization of laminar transient flow regimes and mixing in T-shaped micromixers. *Heat Transfer Eng.* **2009**, *30*, 91.
- (29) Hussong, J.; Lindken, R.; Pourquie, M.; Westerweel, J. Numerical Study on the Flow Physics of a T-Shaped Micro Mixer. IUTAM Symposium on Advances in Micro- and Nanofluidics. Dordrecht, 2009; p 191.
- (30) Minakov, A. V.; Rudyak, V. Y.; Gavrilov, A. A.; Dekterev, A. A. Mixing in a T-shaped micromixer at moderate Reynolds numbers. *Thermophys. Aeromech.* **2012**, *19*, 385.

- (31) Fani, A.; Camarri, S.; Salvetti, M. V. Investigation of the steady engulfment regime in a three-dimensional T-mixer. *Phys. Fluids* **2013**, *25*, 064102.
- (32) Andreussi, T.; Galletti, C.; Mauri, R.; Camarri, S.; Salvetti, M. V. Flow regimes in T-shaped micro-mixers. *Comput. Chem. Eng.* **2015**, *76*, 150.
- (33) Mariotti, A.; Galletti, C.; Mauri, R.; Salvetti, M. V.; Brunazzi, E. Steady and unsteady regimes in a T-shaped micro-mixer: Synergic experimental and numerical investigation. *Chem. Eng. J.* **2018**, *341*, 414.
- (34) Lobasov, A.; Minakov, A.; Kuznetsov, V.; Rudyak, V.; Shebeleva, A. Investigation of mixing efficiency and pressure drop in T-shaped micromixers. *Chem. Eng. Process.* **2018**, *134*, 105.
- (35) Jeong, J.; Hussain, F. On the identification of a vortex. *J. Fluid Mech.* **1995**, *285*, 69.
- (36) Lobasov, A.; Minakov, A.; Rudyak, V. Study of the Mixing Regimes of a Fluid and a Nanofluid in a T-shaped Micromixer. *J. Eng. Phys. Thermophys.* **2018**, *91*, 124.
- (37) Bothe, D.; Stemich, C.; Warnecke, H.-J. Computation of scales and quality of mixing in a T-shaped microreactor. *Comput. Chem. Eng.* **2008**, *32*, 108.
- (38) Lindken, R.; Westerweel, J.; Wieneke, B. Stereoscopic micro particle image velocimetry. *Exp. Fluids* **2006**, *41*, 161.
- (39) Hoffmann, M.; Schlüter, M.; Rübiger, N. Experimental investigation of liquid-liquid mixing in T-shaped micro-mixers using micro-LIF and micro-PIV. *Chem. Eng. Sci.* **2006**, *61*, 2968.
- (40) Soleymani, A.; Yousefi, H.; Turunen, I. Dimensionless number for identification of flow patterns inside a T-micromixer. *Chem. Eng. Sci.* **2008**, *63*, 5291.
- (41) Poole, R. J.; Alfateh, M.; Gauntlett, A. P. Bifurcation in a T-channel junction: Effects of aspect ratio and shear-thinning. *Chem. Eng. Sci.* **2013**, *104*, 839.

- (42) Fani, A.; Camarri, S.; Salvetti, M. V. Unsteady asymmetric engulfment regime in a T-mixer. *Phys. Fluids* **2014**, *26*, 074101.
- (43) Thomas, S.; Ameen, T. An experimental investigation of moderate Reynolds number flow in a T-Channel. *Exp. Fluids* **2010**, *49*, 1231.
- (44) Thomas, S.; Ameen, T.; Guilkey, J. Mixing kinematics of moderate Reynolds number flows in a T-channel. *Phys. Fluids* **2010**, *22*, 1.
- (45) Galletti, C.; Mariotti, A.; Siconolfi, L.; Mauri, R.; Brunazzi, E. Numerical investigation of flow regimes in T-shaped micromixers: benchmark between finite volume and spectral element methods. *Can. J. Chem. Eng.* **2019**, *97*, 528.
- (46) Mariotti, A.; Galletti, C.; Salvetti, M. V.; Brunazzi, E. Unsteady Flow Regimes in a T-Shaped Micromixer: Mixing and Characteristic Frequencies. *Ind. Eng. Chem. Res.* **2019**, *58*, 13340.
- (47) Kockmann, N.; Kiefer, T.; Engler, M.; Woias, P. Convective mixing and chemical reactions in microchannels with high flow rates. *Sensors Actuat. B-Chem.* **2006**, *117*, 495.
- (48) Soleymani, A.; Kolehmainen, E.; Turunen, I. Numerical and experimental investigations of liquid mixing in T-type micromixers. *Chem. Eng. J.* **2008**, *135*, S219.
- (49) Reddy Cherlo, S. K.; Pushpavanam, S. Effect of depth on onset of engulfment in rectangular micro-channels. *Chem. Eng. Sci.* **2010**, *65*, 6486.
- (50) Camarri, S. Flow control design inspired by linear stability analysis. *Acta Mech.* **2015**, *226*, 979.
- (51) Luchini, P.; Bottaro, A. Adjoint equations in stability analysis. *Annu. Rev. Fluid Mech.* **2014**, *46*, 493.

- (52) Sipp, D.; Marquet, O.; Meliga, P.; Barbagallo, A. Dynamics and Control of Global Instabilities in Open-Flows: A Linearized Approach. *Appl. Mech. Rev.* **2010**, *63*, 030801.
- (53) Lashgari, I.; Tammisola, O.; Citro, V.; Juniper, M.; Brandt, L. The planar X-junction flow: Stability analysis and control. *J. Fluid Mech.* **2014**, *753*, 1.
- (54) Chen, K.; Rowley, C.; Stone, H. Vortex dynamics in a pipe T-junction: Recirculation and sensitivity. *Phys. Fluids* **2015**, *27*.
- (55) Chen, K.; Rowley, C.; Stone, H. Vortex breakdown, linear global instability and sensitivity of pipe bifurcation flows. *J. Fluid Mech.* **2017**, *815*, 257.
- (56) Siconolfi, L.; Fani, A.; Camarri, S.; Salvetti, M. V. Effect of geometry modifications on the engulfment in micromixers: Numerical simulations and stability analysis. *Eur. J. Mech. B-Fluids* **2016**, *55*, 360.
- (57) Babu, H.; Satu, S.; Haderlein, M.; Peukert, W.; Verma, N. Numerical investigation of flow patterns and concentration profiles in Y-mixers. *Chem. Eng. Technol.* **2016**, *39*, 1963.
- (58) You, B.; Choi, Y.; Im, S. Influence of adjusting the inlet channel confluence angle on mixing behaviour in inertial microfluidic mixers. *Microfluid. Nanofluid.* **2017**, *21*, 121.
- (59) Mariotti, A.; Galletti, C.; Brunazzi, E.; Salvetti, M. V. Steady flow regimes and mixing performance in arrow-shaped micro-mixers. *Phys. Rev. Fluids* **2019**, *4*, 034201.
- (60) Galletti, C.; Brunazzi, E.; Siconolfi, L.; Spaltro, D.; Mauri, R. Mixing performance of arrow-shaped micro-devices. *Chem. Engineer. Trans.* **2017**, *57*, 1309.
- (61) Mariotti, A.; Antognoli, M.; Galletti, C.; Brunazzi, E.; Salvetti, M. V. Unsteady flow regimes and mixing performance in arrow-shaped micro-mixers. *submitted for publication* **2019**,

- (62) Schikarski, T.; Trzenschiok, H.; Avila, M.; Peukert, W. Influence of Mixing on the Precipitation of Organic Nanoparticles: A Lagrangian Perspective on Scale-up Based on Self-Similar Distributions. *Chemical Engineering and Technology* **2019**, *42*, 1635.
- (63) Gradl, J.; Schwarzer, H.-C.; Schwertfirm, F.; Manhart, M.; Peukert, W. Precipitation of nanoparticles in a T-mixer: Coupling the particle population dynamics with hydrodynamics through direct numerical simulation. *Chemical Engineering and Processing: Process Intensification* **2006**, *45*, 908.
- (64) Batchelor, G. K. Small-scale variation of convected quantities like temperature in turbulent fluid. Part 1. General discussion and the case of small conductivity. *J. Fluid Mech.* **1959**, *5*, 113.
- (65) Ottino, J. Mixing and chemical reactions a tutorial. *Chem. Eng. Sci.* **1994**, *49*, 4005.
- (66) Bothe, D.; Lojewski, A.; Warnecke, H.-J. Fully resolved numerical simulation of reactive mixing in a T-shaped micromixer using parabolized species equations. *Chem. Eng. Sci.* **2011**, *66*, 6424.
- (67) Borgogna, A.; Murmura, M.; Annesini, M.; Giona, M.; Cerbelli, S. A hybrid numerical approach for predicting mixing length and mixing time in microfluidic junctions from moderate to arbitrarily large values of the Péclet number. *Chem. Eng. Sci.* **2019**, *196*, 247.
- (68) Giona, M.; Venditti, C.; Androver, A. On the long-term simulation of stochastic differential equations for predicting effective dispersion coefficients. *Physica A* **In Press**,
- (69) Hinch, E. *Mixing, Chaos and Turbulence*; NATO Science Series B; Springer Berlin, 1999; Chapter Mixing: turbulence and chaos - an introduction.
- (70) Ottino, J.; Wiggins, S. Introduction: Mixing in microfluidics. *Philos. T. R. Soc. A* **2004**, *362*, 923.